International Journal of Geology, Earth & Environmental Sciences ISSN: 2277-2081
An Open Access, Online International Journal Available at http://www.cibtech.org/jgee.htm
2024 Vol. 14, pp. 7-36/Karl
Research Article

EVOLUTION AND DESTRUCTION OF A ROTATING MARINE ENVIRONMENT

Karl Heinz Szekielda*
Fulbright Alumnus, University of the Bahamas
Ateneo University de Manila
**Author for Correspondence: kszekielda@ateneo.edu*

ABSTRACT
The eastern part of the Caribbean Sea is exposed to various source waters that compensate for loss of water by evaporation in the Caribbean Sea. The replacement water is mainly derived from the North Atlantic, the South Atlantic and freshwater contribution from the Amazon and the Orinoco rivers. Some modified South Atlantic water travels northward in form of rings carried by the North Brazil Current. This study estimates, through image interpretation the formation, pathway and destruction of surface ring water that is transported with the Guyana Current towards the Antilles.
The retroflection of the North Brazil Current, the region where ring formation takes place, may translate from its southern position at around 6^0N during summer to a position at late autumn around 9^0N. However, the position of the retroflection may fluctuate once a ring has been released. After separation from the retroflection, the position of a ring fluctuates as well, and the amplitude of ring motion is highest close to the retroflection, but it is reduced once the rings starts to translate away from the retroflection. Image interpretation shows that rings have a lifespan of around 70 to 100 days, and their surface may have a displacement velocity of about 0.15 m s^{-1} upon their arrival close to Trinidad. In addition, formation and translation of rings show temporal and spatial irregularity in ring appearance, and fluctuations in intensity seem to be a common characteristic.
Close to Trinidad, ring water interacts with effluent from the Orinoco River and the resulting mixture enters the passage at the Gulf of Paria and north of Trinidad while another part is transported farther north as surface remnants from the deacaying ring. The northern part of the decaying ring surface may reach the passages between Martinique and Guadeloupe but rarely extends to the latitude of St. Barthélemy. During the decay phase close to Trinidad, open ocean water starts to enter a ring's eastern margin at a velocity of approximately 0.3 m s^{-1}, but the azimuthal speed of surface water can accelerate to about 1.1 m s^{-1} at the western outer periphery of the ring. The inflowing Atlantic water to the Caribbean seems to pressure surface remnants in a westward direction through the passages, but image interpretation shows that the major transport of residual surface ring water appears mainly through the channels south of Guadeloupe and Dominique. After rings stall in the vicinity of Trinidad, there is an indication that destruction of a ring surface can take place within four weeks.

Keywords: *Lesser Antilles, North Brazil Current rings, Formation, Destruction*

INTRODUCTION
The Caribbean Sea has a unique geomorphological setting and the sill depth of the Lesser Antilles controls the water exchange between the Atlantic Ocean and the Caribbean Sea. The southern channels in the island chain are the dominant entries for the water flow to the Caribbean but the seasonal transport shows variations especially through the Windward Islands passages in the southern Caribbean (Stalcup and Metcalf (1972); Wilson and Johns (1997); Johns *et al.*, (1999); Johns *et al.*, (2002)). The different sources of water that compensate the loss of water by evaporation in the Caribbean Sea generate a very complex hydrography because the replacement water is derived from the North Atlantic, the South Atlantic and freshwater contribution from the Amazon and the Orinoco rivers. Furthermore, upwelling

and rings from the North Brazil Current (NBC) contribute water with varying characteristics to the Caribbean Sea.

Atlantic water enters the Caribbean through the major passages in the Lesser Antilles between Grenada, St. Vincent, and St. Lucia, but the transport through the Dominica passage is less (Stalcup and Metcalf, 1972). Studies on the seasonal cycles of the Caribbean passage transports show that changes in the eastern part of the Caribbean Sea are largely related to variations in the Tropical Atlantic in response to the seasonal migration of the Intertropical Convergence Zone and variability in the North East trade wind system (Johns *et al.*, 2002). It is estimated that about half of the water entering the Caribbean Sea originates in the South Atlantic, whereas north of Martinique, the inflow is mainly Gulf Stream water returning southwestward in the North Equatorial Current. The northern inflow passes through the Leeward Islands of the Lesser Antilles, through the Windward Passage between Cuba and Hispaniola, and through the Mona Passage between Hispaniola and Puerto Rico (Richardson, 2005).

Modified South Atlantic water is carried northward by the North Brazil Current in form of rings that translate separately from the main current. Water carried by the rings is characterized by a lower salinity compared to Atlantic water and propagates northwestward until the rings are obstructed by the bathymetry of the Lesser Antilles (Johns et al. (2002); Johns et al. (1990); Richardson et al. (1994); Didden and Schott (1993); Fratantoni et al. (1995); Goni and Johns (2001); Cruz Gómez and Bulgakov (2007)). The contribution of freshwater to the Caribbean Sea is based on the discharge of water from the Amazon and the Orinoco that undergo significant seasonal changes. Both rivers extend their freshwater plume northwestward from August to November, and arrive at the islands about three to four months after the peak of the seasonal rains in northeastern South America (Chérubin and Garavelli, 2016). The surface flow in the vicinity of the Antilles east of 70^0 W shows a separation by a permanent counter-current that flows eastwards, and divides the westward current into a rapid flow in the south and a slower current in the northern half (Duncan *et al.*, 1982). Large fluctuations in current speed are observed in the southern passages in the Lesser Antilles, but their amplitudes are reduced north of Dominica. The variability is caused by the interaction between rings arriving from the equatorial Atlantic and the topography around the Lesser Antilles (Johns *et al.*, 2002). Rings show typically enrichment of chlorophyll around their periphery (Johns et al. (1990); Fratantoni and Glickson (2002)), and they may force coastal water away into deeper regions (Richardson, 2005). However, there are no observations that complete rings enter the Caribbean Sea as a coherent vortex containing the same core properties as an incident ring (Fratantoni and Richardson, 2006). That means that the water entering the passages in the south of the Lesser Antilles seem to be mainly remnants from rings and effluent from the Orinoco. In the Venezuela Basin, dominant upwelling is observed at 63^0 to 65^0W and 70^0 to 73^0W that provide additional nutrients to the surface water and subsequently to plankton development (Müller-Karger et al. (1988); Müller-Karger et al. (1989); Hu et al. (2004); Rueda-Roa and Müller-Karger, 2013)). Upwelling along the northern coast of Trinidad is not well covered in the literature but it seems to be a distinct regime because it appears to be separated from the western upwelling region by the discharge of the Orinoco and Essequibo water passing also through the Gulf of Paria (Wilson, 2008, Del Castillo *et al.*, 1999). Consequently, seasonal cycles in river discharge, ring translation and the demise of rings determine the hydrographic field in the vicinity of the Lesser Antilles. Although North Brazil Current rings (NBC-rings) are well documented, the biological and chemical processes that take place during the development and degradation of rings are complex due to the marine ecosystem that develops at a different spatial-temporal scale compared to physical and chemical processes. In addition to the complex hydrography around the Lesser Antilles, the region shows a regional anomaly in sea surface temperature with a slight cooling. Both day and night measurements over twenty years show a decrease in sea surface temperature of around -0.004 ^{0}C y^{-1} to -0.002 ^{0}C y^{-1} in the vicinity of Dominica (Szekielda, 2023). Comparable long-time observations by NASA (no year) in the eastern Caribbean Sea confirm that the Lesser Antilles region is exposed to a temperature anomaly.

The biological impact of Amazon water carried by NBC-rings was recognized when in 2009 a large influx of Amazon River into the northeastern Caribbean Sea changed a large area to low surface salinity

of about 35.8 psu with an elevated surface temperature and high chlorophyll to about 1.3 mg m^{-3} (Johns *et al.*, 2014). Thus, this region is challenging to better understand the dynamics and anomalies with respect to eutrophication and the distribution pattern of the biological system. In particular, additional information on the development and decay of NBC-rings is beneficial for a better understanding of the ecosystem in NBC-rings and their impact on the marine environment. Therefore, the motivation for this study is to estimate the formation, pathway and demise of NBC-rings and to distinguish between the different surface waters in the vicinity of the Lesser Antilles. As current speed and ring displacement are in the neighborhood of centimeters to meters per second, fast changes in surface characteristics can be anticipated. Such changes are difficult to monitor with conventional ship surveys, therefore the study is based on remotely sensed chlorophyll and temperature measurements that were accessed through two sources.

MATERIALS AND METHODS

The first used data set is accessed via the Worldview from NASA's EOSDIS that has the capability to interact through <https://worldview.earthdata.nasa.gov>. The second source is also based on satellite remotely sensed temperature and chlorophyll concentrations that were processed with Giovanni, a system for multidisciplinary research and applications that was accessed via https://giovanni.gsfc.nasa.gov/ (Acker and Leptoukh, 2007). The area of investigations is shown in Figure 1 with the various sub-sections to address specific tasks.

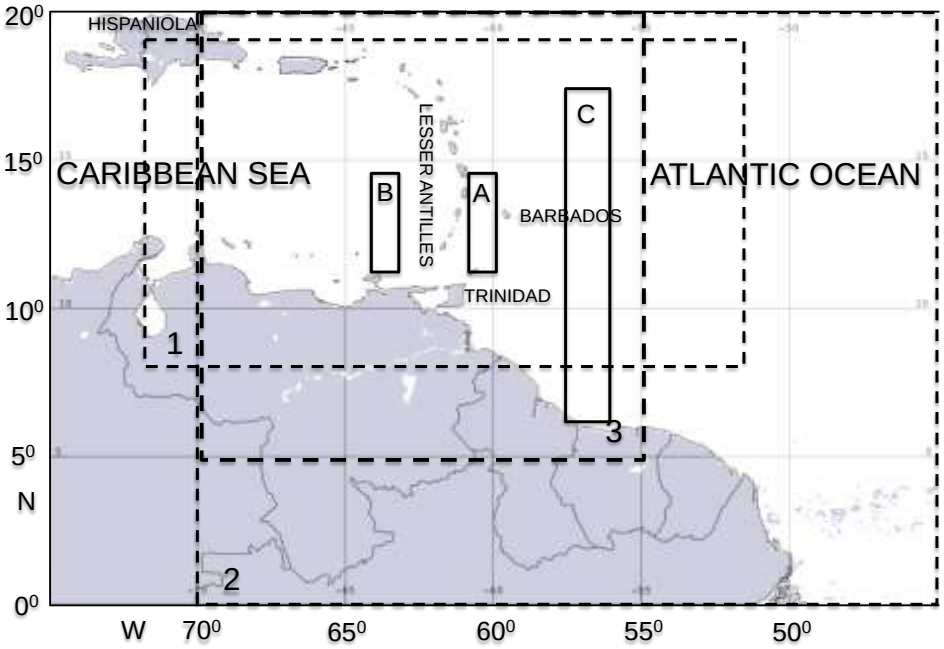

Figure 1: Location of the research areas: Site 1 is located at 8^0N, 52^0W and 19^0 N, 72^0N; Site 2 is located at 0^0N, 45^0W and 20^0N, 70^0W; Site 3 is located at 5^0N, 55^0W and 20^0N,70^0W; Site A is east of the Lesser Antilles and is located at 11^0N, 60^0W and 14^0N, 61^0W; Site B is west of the Lesser Antilles and is located at 11^0N, 63^0W and 14^0N 64^0W; Site C is located at 6^0 N, 57^0 W and 18^0N, 56^0 W.

Chlorophyll measurements were used for characterizing variations in optical water properties. However a cautious note is necessary because of the interference of material other than chlorophyll on the standard algorithm to estimate chlorophyll concentrations. Although in the following, the basic parameter is based

on the chlorophyll algorithm, it is occasionally referred to in the text as ocean color when the differentiation between Case 1 and Case 2 water was questionable. This decision is based on the comparison of chlorophyll concentrations and sea surface temperature as shown in Figure 2, where unrealistic high chlorophyll concentrations appear as clusters especially in waters that can be related to the Orinoco and Amazon discharge and NBC-rings. Although unrealistic, those high values can serve as a parameter to distinguish coastal and riverine water (Case 2 water) from those that may carry only living planktonic matter (Case 1 water). However, the figures and legends in the following will refer to chlorophyll concentrations.

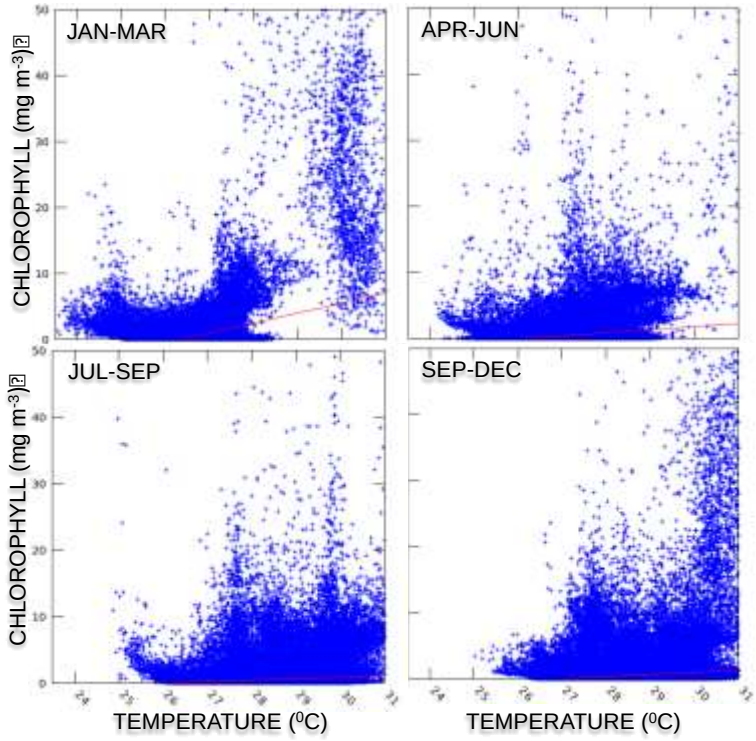

Figure 2: Scatter diagrams of chlorophyll concentrations and temperature for different seasons in 2022 for Site 1 in Figure 1 that is located at 8^0N, 52^0W and 19^0 N, 72^0N.

RESULTS AND DISCUSSION

General description of the investigated region

The average distribution of temperature and chlorophyll concentrations in the eastern Caribbean Sea reveals the basic hydrography in the vicinity of the Lesser Antilles as shown in Figure 3. Low temperatures, especially along the coasts of Venezuela, indicate the upwelling regimes, and the warm water illustrates the impact of southern Atlantic water up to Trinidad and Tobago. The North Atlantic water borders with relatively colder temperature in the northern part of the Lesser Antilles, and the leeward side of the island chain, shows the warming effect of wakes on surface temperature that has been reported previously (Szekielda, 2023). The complexity of surface waters in the investigated region is indicated by extremes in their physical and chemical composition, expressed in elevated chlorophyll concentrations in regions where eutrophication due to upwelling and/or river effluent is present.

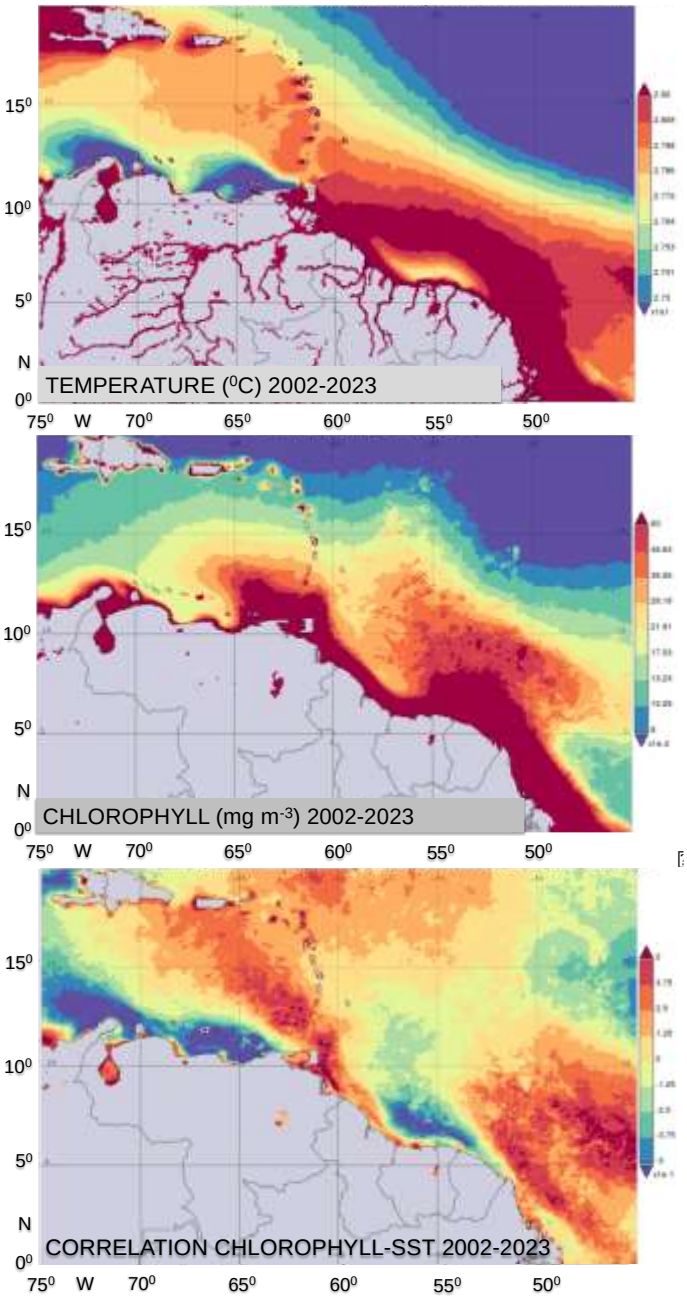

Figure 3: Temperature (^{0}C), chlorophyll concentrations (mg m^{-3}) and correlation of temperature with chlorophyll for 2002 to 2023. The site is located at 0^{0}N, 45^{0}W and 20^{0}N, 75^{0}W and covers the whole area outlined in Figure 1.

The correlation of temperature and chlorophyll in Figure 3 provides information on the major processes of surface waters that include the spreading of coastal water from the south. The outflow of the Orinoco River east of Trinidad is discernable and the transport of plume water, after entering the passages south of St. Vincent, can be tracked up to Puerto Rico. At around 8^{0}N, the boundary of the retroflection is depicted by low correlation, but a strong negative correlation between temperature and chlorophyll is found at

around 55^0N that is indicative for the existence of upwelling and is in agreement with the low temperature distribution in the same region.

The surface salinity distribution in Figure 4 shows the influence of Amazon water with lower salinity stretching to the east of the Lesser Antilles. This is interpreted as a result of rings that, after translating from the south, are observed to be quasi stagnant at around 12^0 to 18^0N. Therefore, ring water or its remnants would cause in the average lower salinity compared to those of Atlantic surface water.

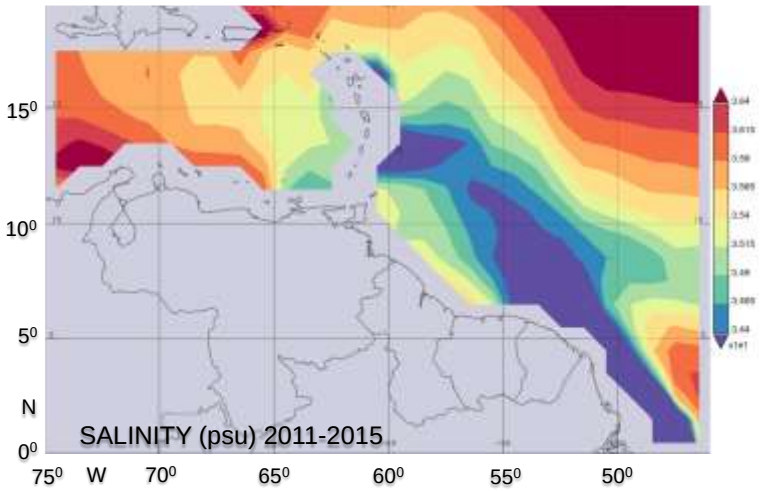

Figure 4: Distribution of salinity based on averaged data from September 2011 to June 2015. The site is located at 0^0N, 45^0W and 20^0N, 75^0W and covers the whole area outlined in Figure 1.

North Brazil Current-ring formation

Ring formation starts in the area where the North Brazil Current retroflects and feeds into the North Equatorial Countercurrent. Rings may form throughout the year on the western side of the retroflection that is associated with the northward extension of the NBC in early fall and winter (Lumpkin and Garzoli *et al.*, 2003; Fratantoni and Richardson, 2006). As shown with Figure 5, the retroflection is not stationary because it moves from its southern position at around 6^0N during summer in a northwest direction, and in late autumn, it is positioned around 9^0N where it stays until the beginning of the following year.

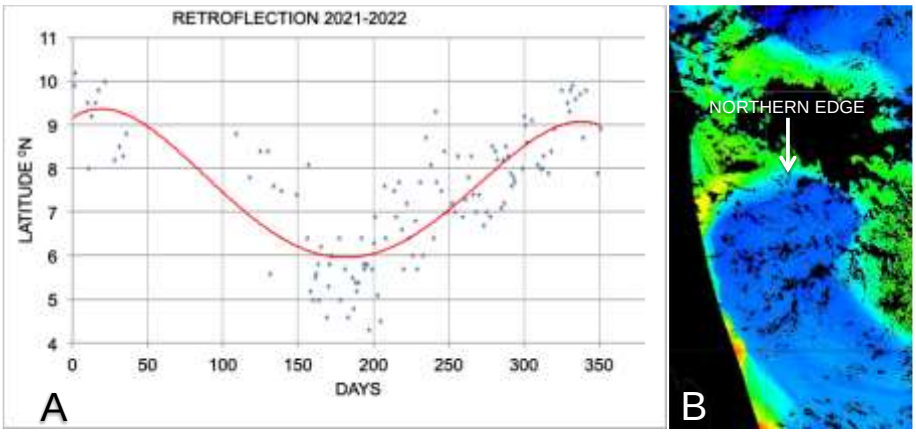

Figure 5: A: Estimated location of the northern edge of the retroflection. The red line shows the 4th polynomial trend line. B: Principle used to identify the northern edge of the retroflection in EOSDIS images.

Ring formation was observed on 15 January 2024 when two rings were already in existence and one ring was under development as shown in Figure 6. Each ring was formed within a time frame of about four weeks. Ring A was generated at the beginning of December 2023, diverted in a northward direction, passing Barbados, and extending its outer periphery to the longitude of Martinique.

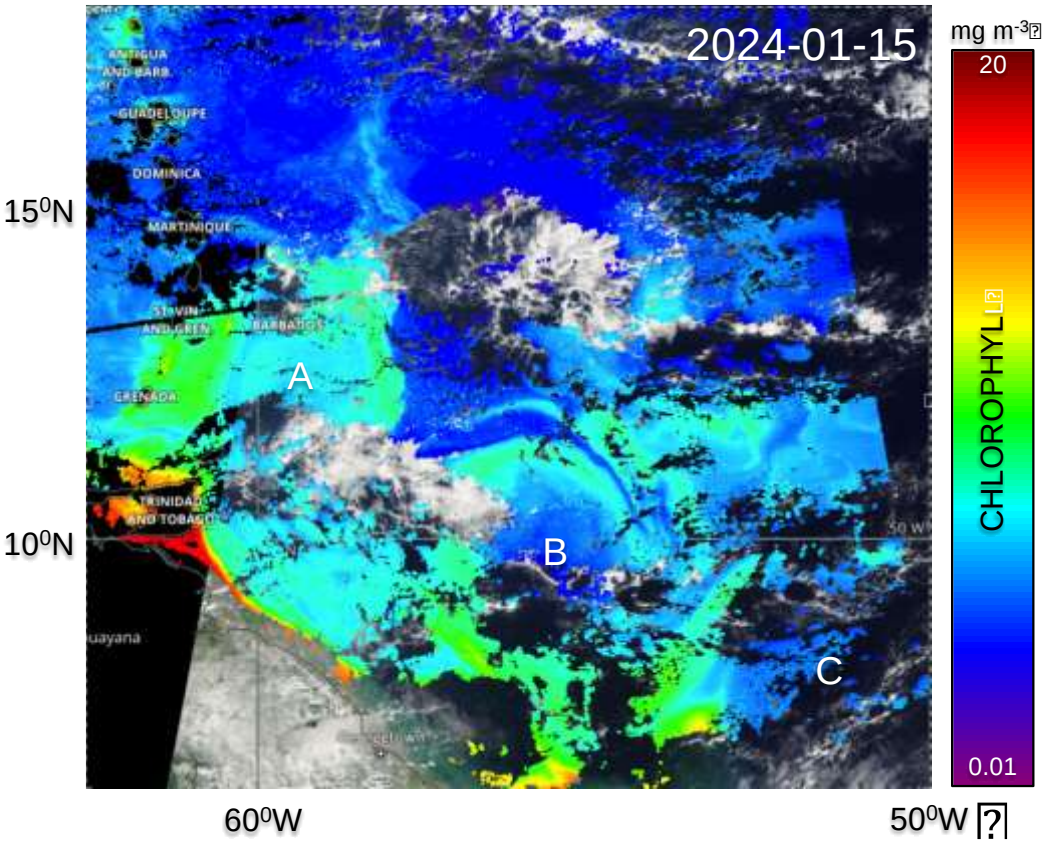

Figure 6: Tracking of rings A and B. The new ring C developed and became detached from the retroflection around 15 January 2024. The color bar is an approximation of chlorophyll concentrations in EOSDIS imagery.

Research in the past dealt with tracking of rings and focused on their internal structures. However, not much is documented on details of ring formation and the time and location at which NBC-rings separate from a retroflection. A time series for December 2023 provides information on the spatial-temporal characteristics of ring formation of which selected images are shown in Figure 7. The retroflection reached on 14 December 9^0 24'N and moved by 12 December to 9^0 42'N. A well-defined ring separated on 26 December from the retroflection as seen in image 3 in Figure 7. The ring started to translate on 29 December, and the retroflection began to move back to 7^0 54'N but returned to 8^0 24'N on 31 December. A new ring developed on 12 January 2024 (not shown in Figure 7) and was located at 7^0 54'N and 51^0W. This development indicates that a newly formed ring may not move northwest for some time after separation from the retroflection, and it also shows that the retroflection may oscillate back south after a ring has been released.

The color gradients in the outer periphery of rings also reveal that once they are generated, they have well-defined and sharp boundaries. However, they carry entrapped coastal water in their outer margin and during their translation, they accumulate more in the outer margin and develop a color change between

ring water and adjacent ocean water. Furthermore, due to the high nutrient content in coastal waters, the outer edge of a ring supports plankton development that further changes the color appearance of the outer periphery.

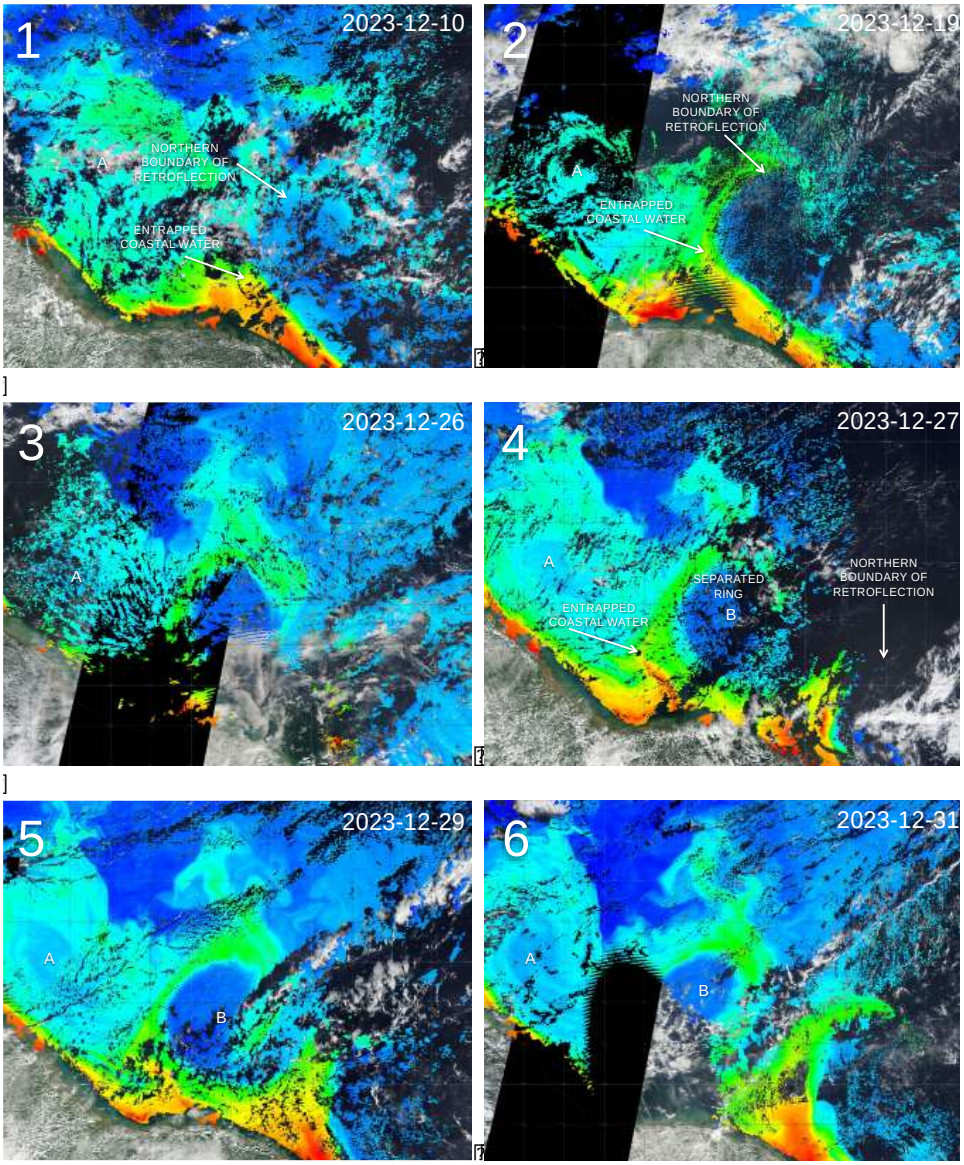

Figure 7: Ring formation observed with EOSDIS from 10 December to 31 December 2023. The images cover the same area as the image in Figure 6.

As shown in Figure 8, the incorporation of coastal surface water into the outer periphery of rings starts during their evolution at the retroflection and is a component for ring construction. Uptake of coastal water is a continuous process during the translation of rings as long as their outer loop reaches coastal water. The example in Figure 8 shows a sequence of a developing ring on 14 December 2023 with the incorporation of coastal water into the retroflection. Ten days later, the separated ring shows additional

coastal water assimilated by the outer ring circulation but the entrapped coastal water loses quickly its signature due to dilution, loss of suspended solids, and because of nutrient supply by coastal water, increase in productivity is conceivable.

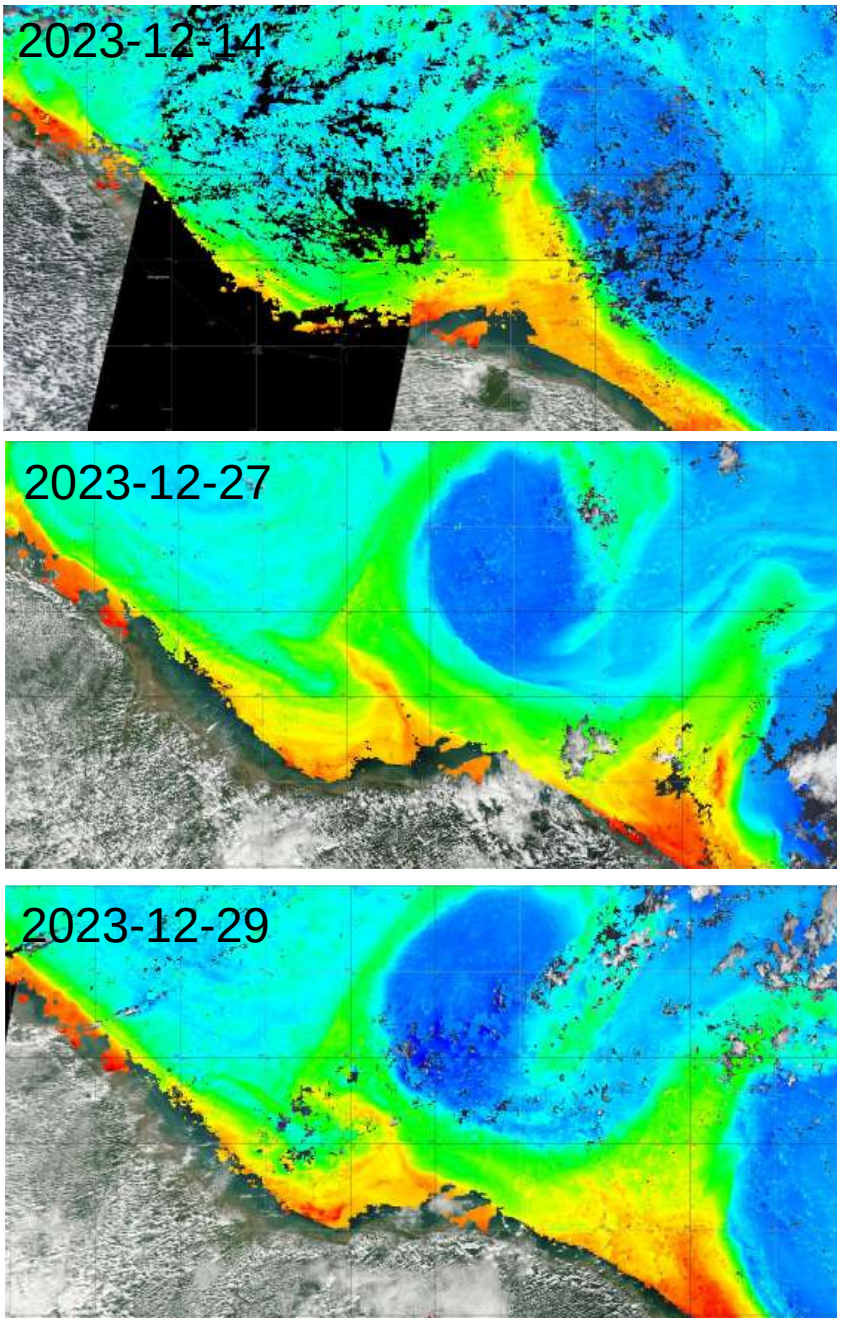

Figure 8: Incorporation of coastal surface water at the retroflection and at the outer periphery of a ring after separation from the retroflection.

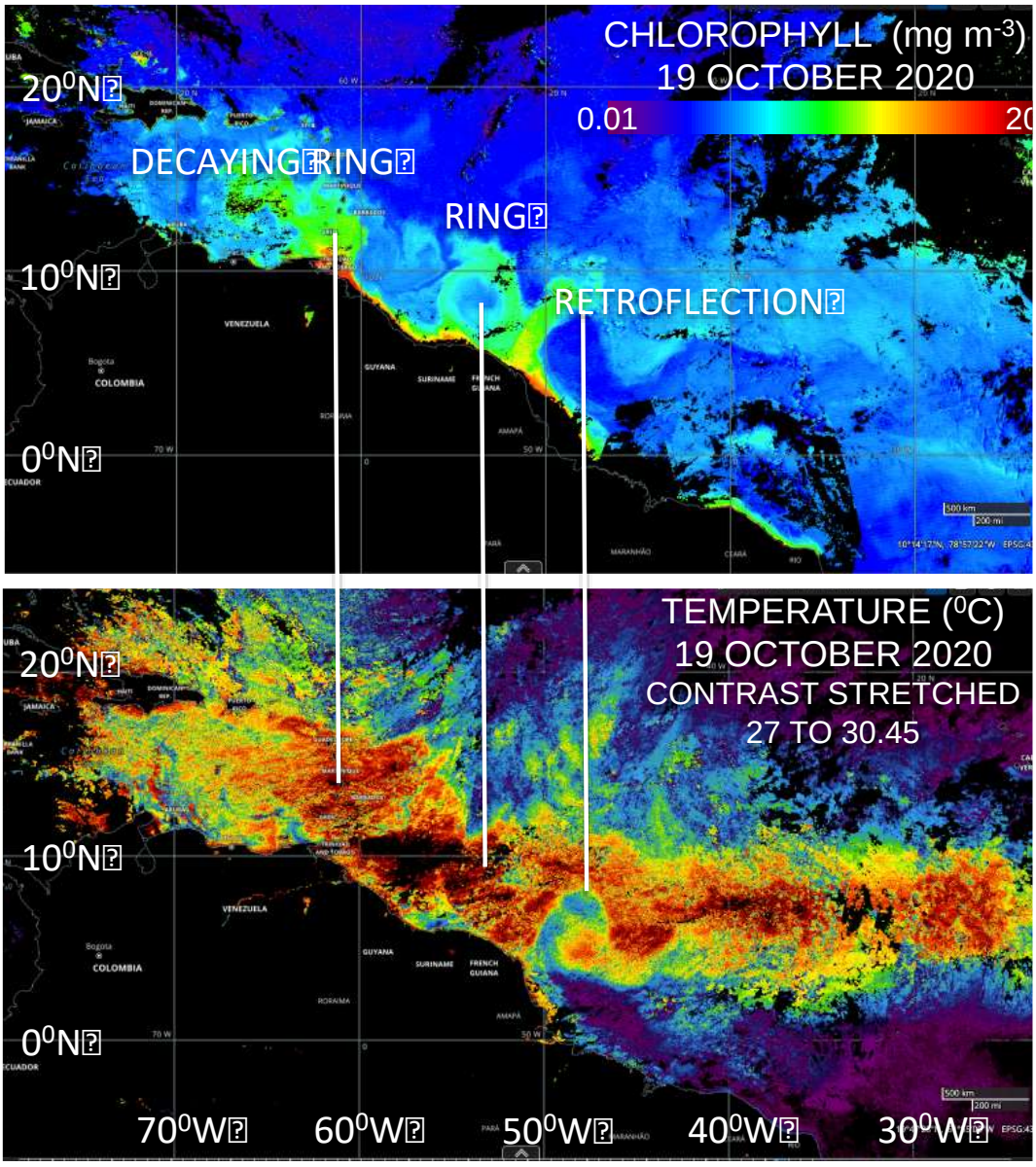

Figure 9: Chlorophyll concentration and temperature distribution on 19 October 2020 show ring formation at the retroflection, an isolated ring and the region of a decaying ring. The temperature image has a contrast stretch for temperature from 27.0⁰ to 30.45⁰C.

Ring propagation

Daily observations of cloudfree coverage is a challenge of opportunity, but unusual cloud conditions allowed to view the different phases of ring appearance as shown in Figure 9. The retroflection is characterized by the sharp color gradient that is generated by the entrapment of coastal and Amazon water in the ring periphery. It also shows a ring that is separated from the retroflection. The corresponding temperature distribution shows that the center of the rings are not well characterized by temperature compared to the color boundaries in the outer ring because of equal surface warming of ring and adjacent

surface water. The ring adjacent to the retroflection started separation from the retroflection around August 25 and was fully separated on 2 September with its center point at 7°21'N, 51°16'W. The ring stalled at the beginning of December at 8°06N, 56°06'W and started to decay around 5 December from this position. This indicates a life span for this ring of approximately 100 days, and considering a straight line of ring displacement from its origin to the location of disintegration, implies only a velocity of about 0.1 m s^{-1}.

After separation from the retroflection, it was observed that some rings oscillate slightly in north-south direction and this change in position of rings is most probably an effect of approaching equatorial waves. This hypothesis is suggested by a general view of ring movement as shown in Figure 10 that is based on the position of the ring center point shortly after complete separation from the retroflection. It shows that the amplitude of ring motion is highest close to the retroflection but it reduces its amplitude with distance from the retroflection.

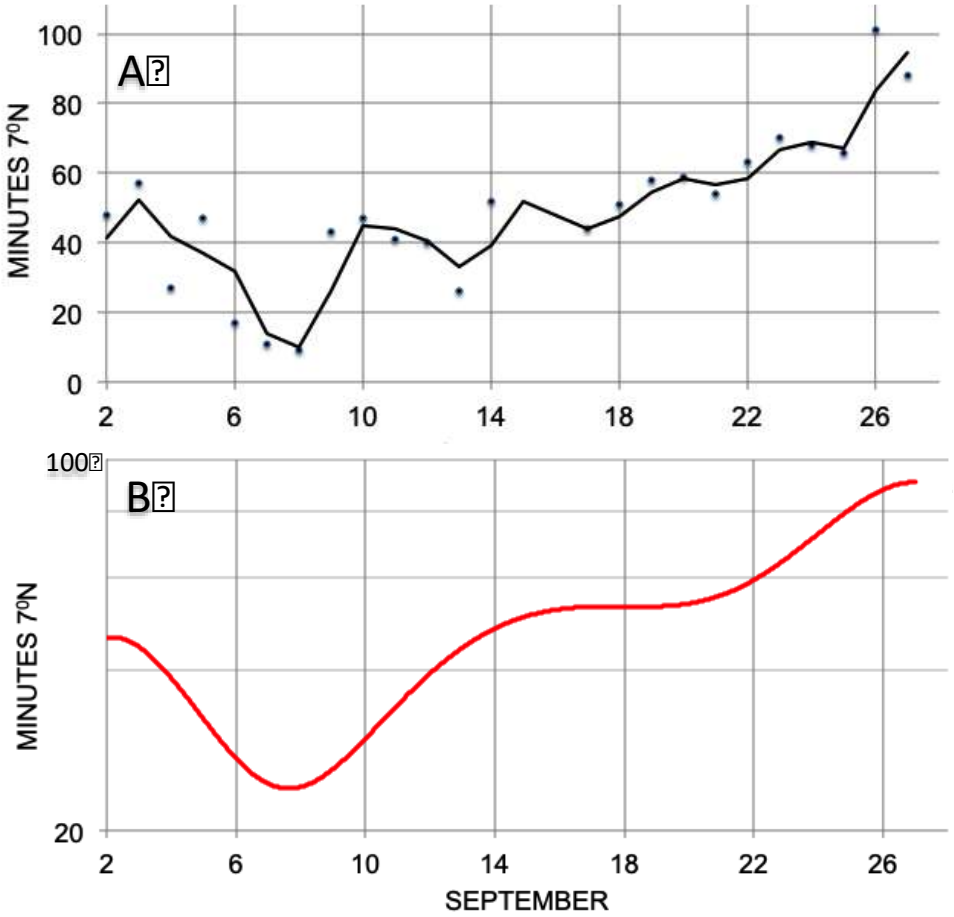

Figure 10: Ring observation in September 2020 on the north-south motion based on the location of the ring center in minutes north of 7^0N. Figure A shows the data points with a two-period moving average. Figure B shows the same data set as in Figure A but with a polynomial fit.

As complete cloudfree conditions are rare, tracking of rings has to apply multi-day composites of which the best alternative at present is an eight-day composite, but even at this temporal resolution, complete coverage of an area is occasionally still limited. Keeping these restrictions in mind, the following application of eight-day composites are used to identify the pathway of NBC-rings from their place of

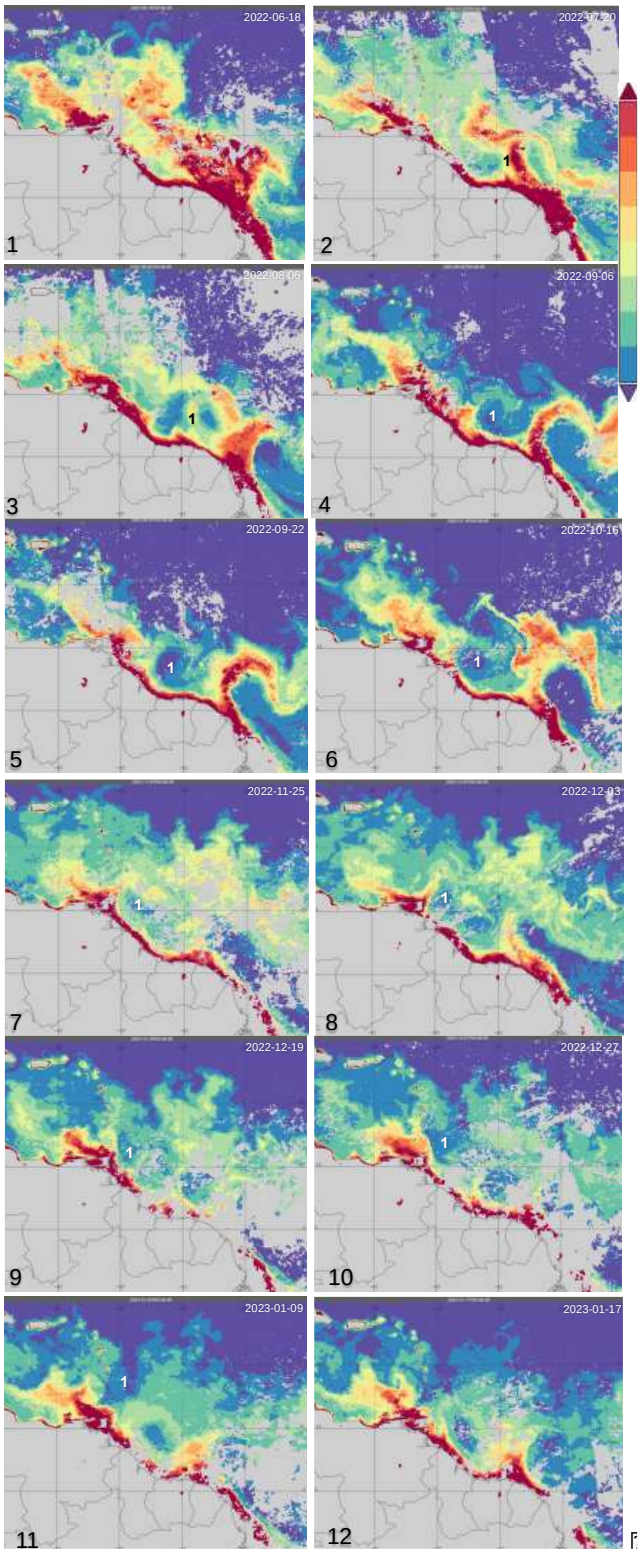

Figure 11: Chlorophyll concentration (mg m^{-3}) based on an eight-day average at 4 km-resolution from18 June 2022 (Image 1) to 17 January 2023 (Image 12). The images are located at 0^0N, 45^0W and 20^0N, 70^0W and their positions are shown in Figure 1 as Site 2.

formation to the place of their decay in the vicinity of the Lesser Antilles. One sequence of observations is shown in Figure 11 that ranges from 18 June 2022 to 17 January 2023. The retroflection is not well recognized in June/July and chaotic distribution of chlorophyll was observed, whereas the image on 25 August shows clearly the retroflection and also shows the separation of a ring (Ring 1) with its center at $7^0$54'N, $53^0$46'W. The ring moved only slowly in a northwest direction, and on 14 September 2022 was at 8°18'41"N, 55°31'35"W and had low chlorophyll concentrations in its center. The ring translated towards the north and once reaching the Lesser Antilles, it started to decay in December.

Figure 12 shows during favorable cloud conditions a comparison of a ring at different temporal and spatial resolutions. Figure 12A gives the 8-day average around 14 September with Ring 1 of which the development is shown in Figure 11. The real-time image in Figure 12B provides details on the entrainment of coastal water into the outer periphery of the ring and its incorporation into the azimuthal surface circulation. The ring seems to be rather stationary at this phase of evolution, and that would explain also, the good agreement between averaged data and the real-time image.

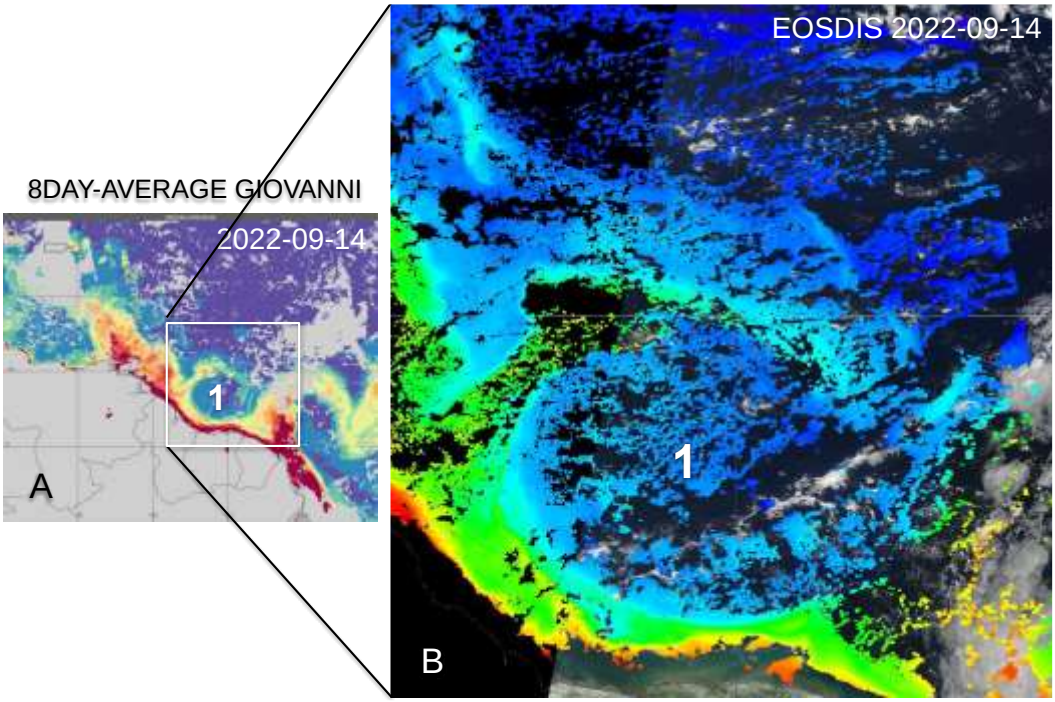

Figure 12: Comparison of eight-day composite (A) at 4km-resolution and one-day coverage of chlorophyll concentrations; (B) at 1km-resolution on 14 September 2022. The image in Figure A is located at 0^0N, 45^0W and 20^0N, 70^0W and its position is shown in Figure 1 as Site 2. The white square in 12A shows the region covered by the EOSDIS image in Figure 12B.

Additional tracking of rings cover the period from 25 January 2023 to 2 June 2023 and is shown in Figure 13. Image 1 in Figure 13 shows a ring that is annotated as A, and a second ring in the stage of formation at the retroflection, is annotated as B. On 10 February, while being close to the Lesser Antilles, Ring A lost its surface expressions around 6 March and eventually disintegrates. Ring B translates after its formation on 14 March, but it lost in May its surface signature as a ring. The destruction of this ring seems to be based on an interaction with another ring that evolved around 14 March and was fully recognized as Ring C on 7 April. The interaction of both rings starts on 6 March and is well recognized on 14 March. Image 6 in Figure 12 shows that Ring C forces Ring B in a north direction as is indicated in

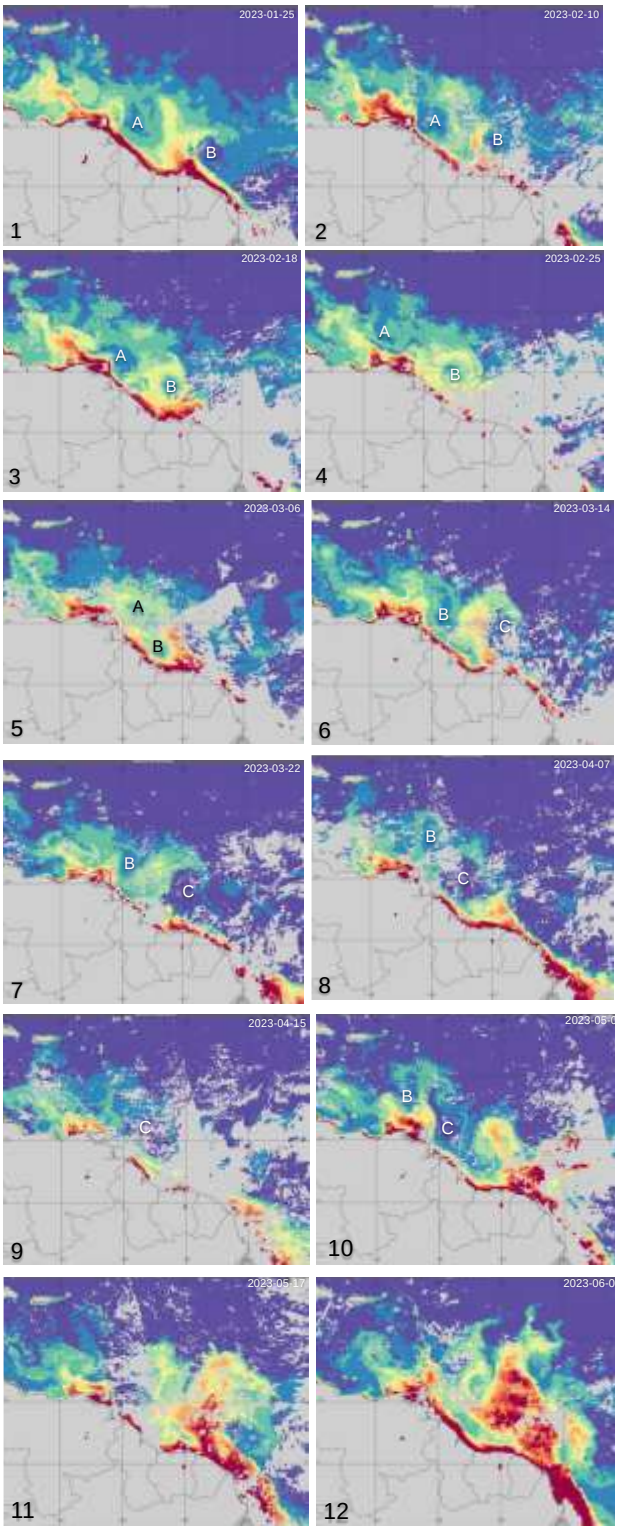

Figure 13: Chlorophyll concentration (mg m^{-3}) based on an eight-day average at 4 km resolution from 25 January 2023 to 2 June 2023. The images are located at 0^0N, 45^0W and 20^0N, 70^0W, and their positions are shown in Figure 1 as Site 2.

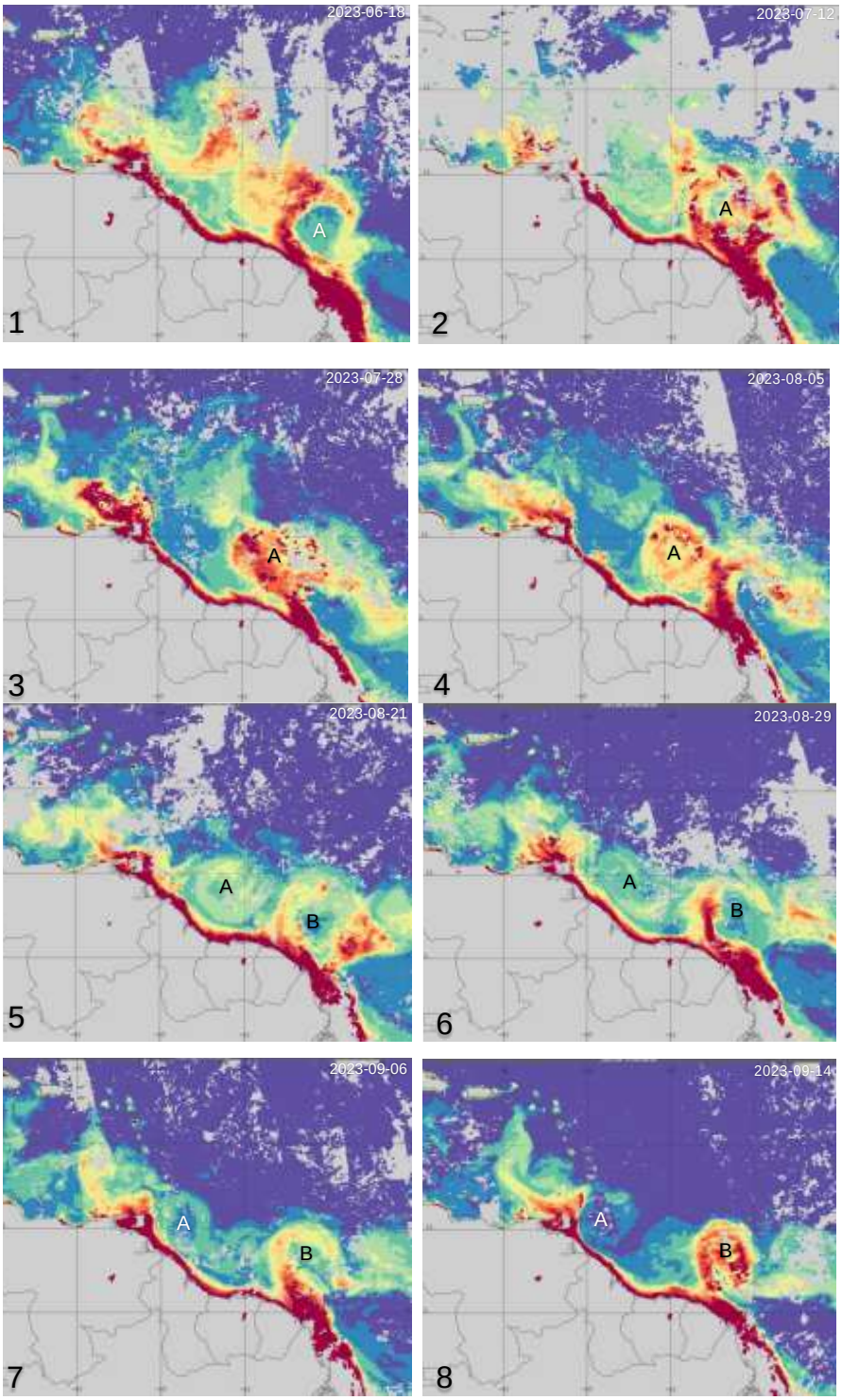

Figure 14: Chlorophyll concentration (mg m^{-3}) based on an eight-daily average at 4 km resolution from 18 June 2023 to 14 September 2023. The images are located at 0^0N, 45^0W and 20^0N, 70^0W, and their positions are shown in Figure 1 as Site 2.

image 8, but both rings lose their surface ring appearance as shown in image 10 on 1 May. Images 11 and 12 show that no further ring formation was observed and that the distribution of ocean color at this time

starts to be rather chaotic. The above described sequence of ring observations show for Ring B an estimated lifespan of 70 to 80 days. Assuming a distance of roughly 1000 km from about 8°N, where formation of the ring was recognized to be at a the position between Trinidad and Barbados, Ring B would have had a displacement velocity of about 0.15 m s^{-1}.

During June to September 2023, another series of images shows the formation, translation and decay of a ring, shown in Figure 14. Ring A formed around 18 June and was completely separated from the retroflection between 28 July and 5 August and translated north, but the ring lost the strong surface color gradient at its arrival in the vicinity of Trinidad and Barbados where it could hardly be recognized. Another ring developed that is annotated as B in the retroflection. The observation with real time data through EOSDIS showed that this ring separated from the retroflection on 21 September 2023.

Ring route through the translation corridor

Rings move in a northwest direction after their separation from the retroflection. The incorporation of coastal water in the outer periphery of rings affects especially the spectral properties that facilitate the recognition of rings when they pass through the translation corridor. Looking further into the performance of rings passing through a corridor, a section perpendicular to the axis of a ring translation corridor, between 6^0N and 18^0N, was analyzed with Hovmöller longitude-averaged salinity and chlorophyll measurements. The salinity distribution is shown in Figure 15 and covers the period September 2011 to May 2015. Although the data are limited to a three-year coverage and measured at a coarse resolution of about 100 km, the seasonal changes in salinity gradients are significant. They are attributed to transport of freshened surface water that is noticeable particularly between 8^0N and 17^0N. The intrusion of freshened surface water is further magnified at higher temporal resolution that is shown in Figure 15B for 2013 to 2014. The lower salinities in the offshore regime are interpreted as an indication for ring occurrence that is also conclusive from the chlorophyll distribution.

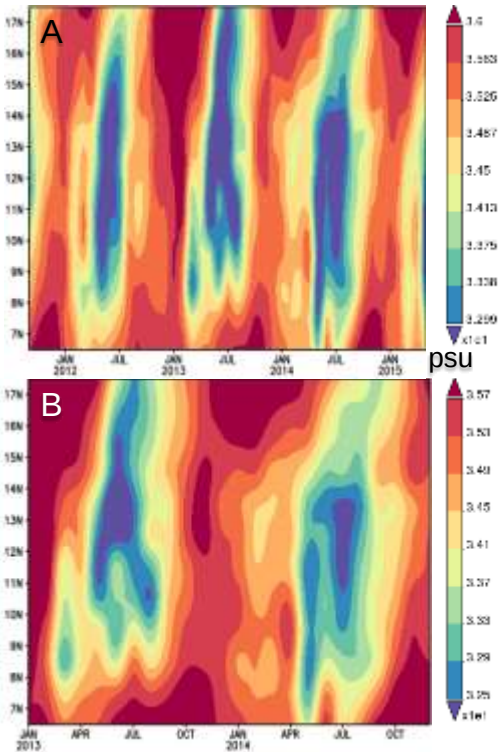

Figure 15: A: Hovmöller longitude-averaged salinity (psu) distribution for September 2011 to May 2015. B: Extended view of figure A from January 2013 to December 2014. Both figures refer to Site C as shown in Figure 1 at 6^0 N, 57^0 W, 18^0N and 56^0 W. The resolution of the salinity measurements is 100 km.

The Hovmöller longitude-averaged chlorophyll distribution as shown in Figure 16 documents that rings or ring remnants passed through the selected region and are the cause for heterogeneity in the chlorophyll distribution. Temporal and spatial irregularities in intensity have been recognized especially between 2009 and 2010, 2019 and 2022. The years 2007, 2009 and 2010 likewise show anomalous distribution and high values that stretches farther north up to18^{0}N. Strong fluctuations are observed in the coastal water from 6^{0}N to 7^{0}N that displays periodic extensions towards the offshore region, and these extensions are captured at the southwestern flank of NBC-rings. Though the coastal water is separated by a strong color gradient from the rings, the presence of filaments in the offshore direction show a link to the outer periphery of ring water. This has been further studied at higher temporal resolution as shown in Figure 17.

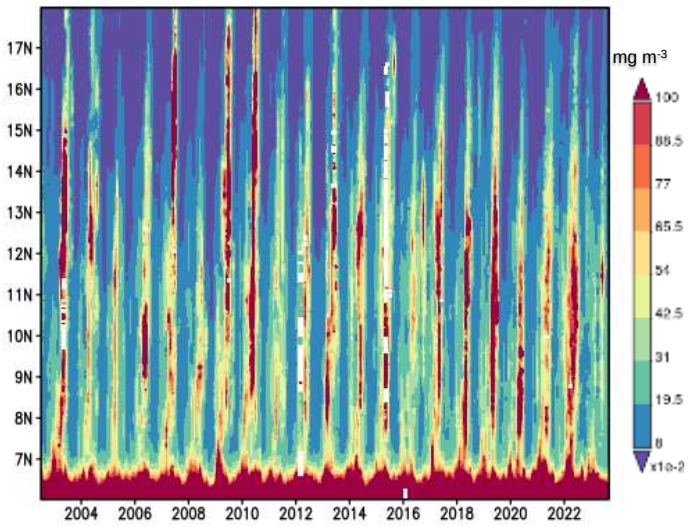

Figure 16: Hovmöller longitude-averaged chlorophyll (mg m^{-3}) 2002-2023 at site C that is shown in Figure 1 at 6^0 N, 57^0 W, 18^{0}N, 56^0 W.

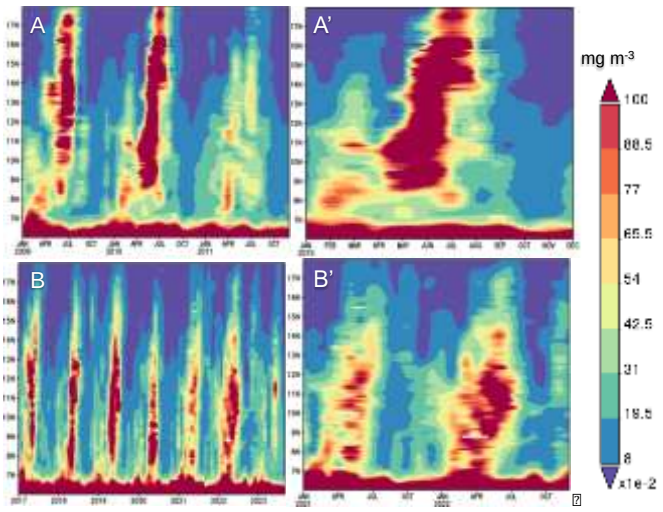

Figure 17: Higher temporal resolution of chlorophyll distribution as shown in Figure 16. The region covers 6^0 N, 57^0 W, 18^{0}N, 56^0 W and is shown as Site C in Figure 1. Figure A covers the years 2009 to 2011 and A' is an extended view for 2010. Figure B covers 2017 to 2023 and Figure B' covers 2021 to 2022.

The near-shore color distribution is displayed with two examples in Figures 17A and B. Corresponding Figures 17A' and B' are presented at higher temporal resolution and cover a shorter time interval. It is evident that the highest color values are restricted to coastal water but that filaments may reach the outer periphery of rings. Consequently, it can be concluded that rings may capture during their translation, coastal water on the southwestern side of rings and may interact with the near-shore circulation. This has been further documented with observations on ring interaction with coastal water, shown in Figure 18.

Ring interaction with coastal water

Figure 18 covers the same region as the one shown in Figure 16 except for the latitude that extends from 6°N to $7^0$30'N with the aim to emphasize the observations on coastal water. This water has the characteristics of Case 2 water as evidenced by the anomalous high values in ocean color. Maximum peaks appear seasonally but with smaller spikes superimposed on them of which neither intensity nor the frequency are periodic. While the spectral response of the outer periphery in rings is based on the entrapment of costal water, the heterogeneity in the coastal regions seems to relate more to the disturbance of near-coastal currents by approaching rings. A rough estimate of ring progression can be made from the Hovmöller analysis under the assumption that the heterogeneity in ocean color is a result of rings passing through the investigated site. This estimate shows that about three to four rings per year could pass through the investigated region.

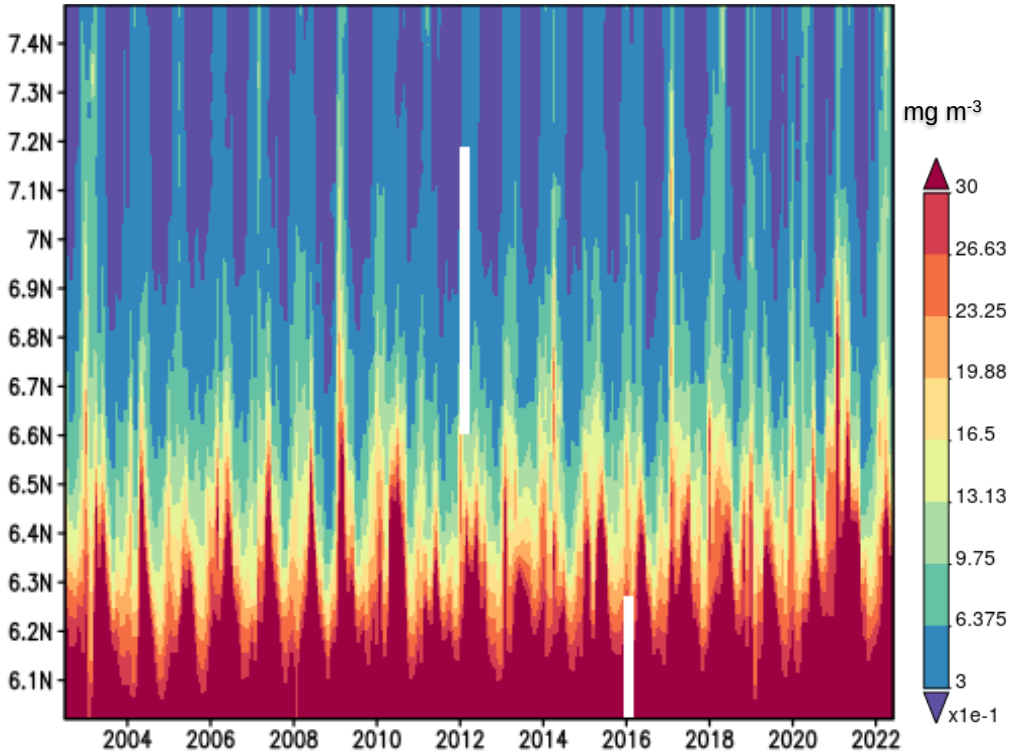

Figure 18: Extended view of coastal water between 6^0 N and 7^0N. Chlorophyll distribution for 2002 to 2022 covers the region 6^0 N, 57^0 W, 7^0 30'N, 56^0 W.

Figure 19A shows an expanded view of Figure 18 for the time scale 2017 to 2023 in Figure 19A, for 2020 to 2021 in Figure 19B, and for 2021 in Figure 19C. Image interpretations showed that the coastal water

fluctuates in patches and that the maximum concentrations drift in a northwest offshore direction, as indicated by the dashed white line in Figure 19C.

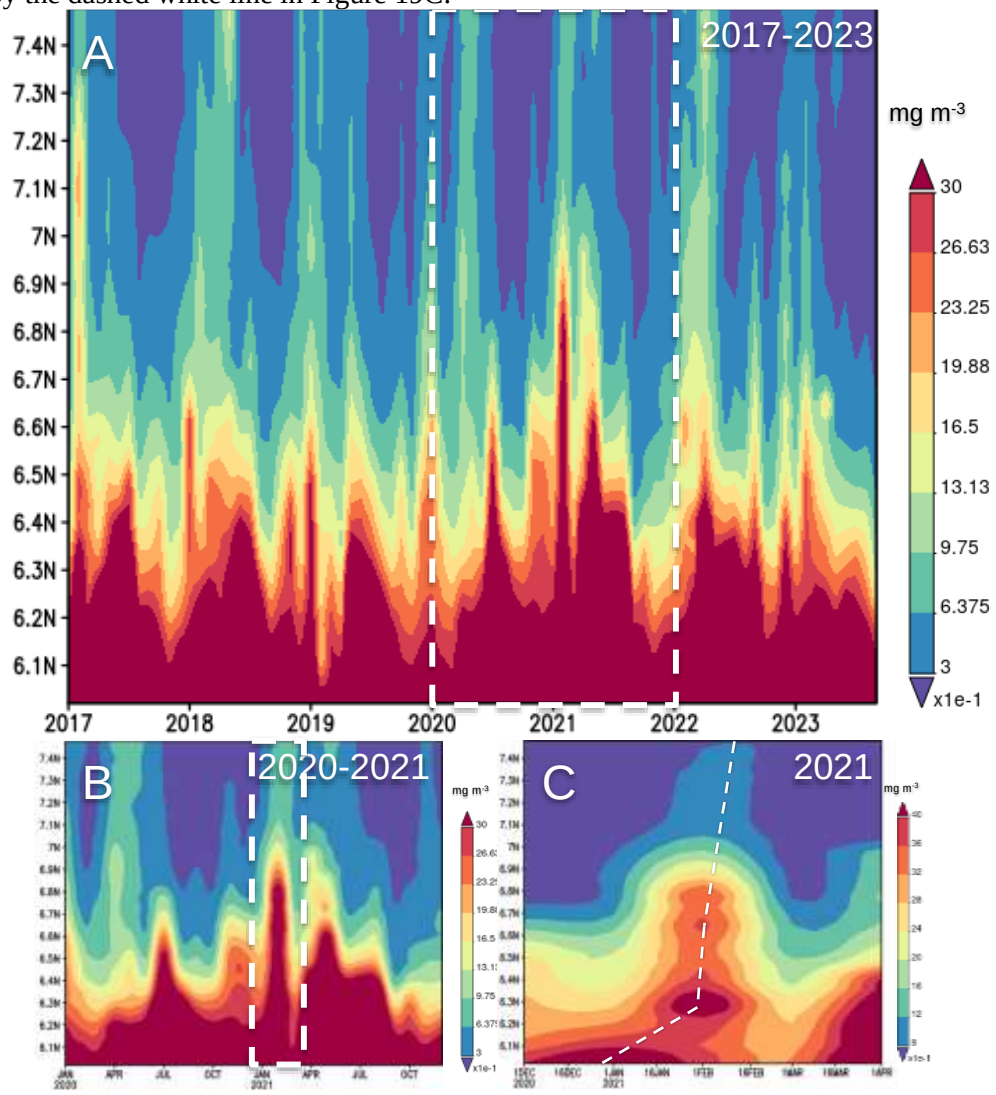

Figure 19: Extended view of coastal water between 6^0 N and 7^0N for January 2017 to December 2023 in Site C of Figure 1 that covers the region 6N, 57W and $7^0$30'N, 56W. The rectangle in Figure 19A coverage for Figure 19B; the latter indicates with the rectangle the coverage for Figure C.

Rings and ring remnants at the Lesser Antilles passages (sections A and B in Figure 1)

Major surface changes appear east of the Lesser Antilles upon arrival and subsequent destruction of NBC-rings. These changes have been analyzed with two sections that are located east and west, respectitvely, and are shown in Figure 1 as site A and site B. In order to study the performance of rings near the Lesser Antilles, one section east of the Lesser Antiles was analyzed to survey the decay of rings with Hovmöller longitude-averages. The results for a nineteen-year long chlorophyll series is shown in Figure 20A and shows the aperiodic advent of chlorophyll maxima. A strong anomaly was found in 2010 that is shown in an extended view in Figure 20B and documents the maximum chlorophyll concentrations around June-July. Further expanded views shown in Figures C and D reveal the heterogeneity and patchy chlorophyll distribution through the section. Figure 20D shows that the chlorophyll concentrations are in a large patch

that migrated in 2010 through this section, and it was most probably the effect from a ring with its center around 12^0N.

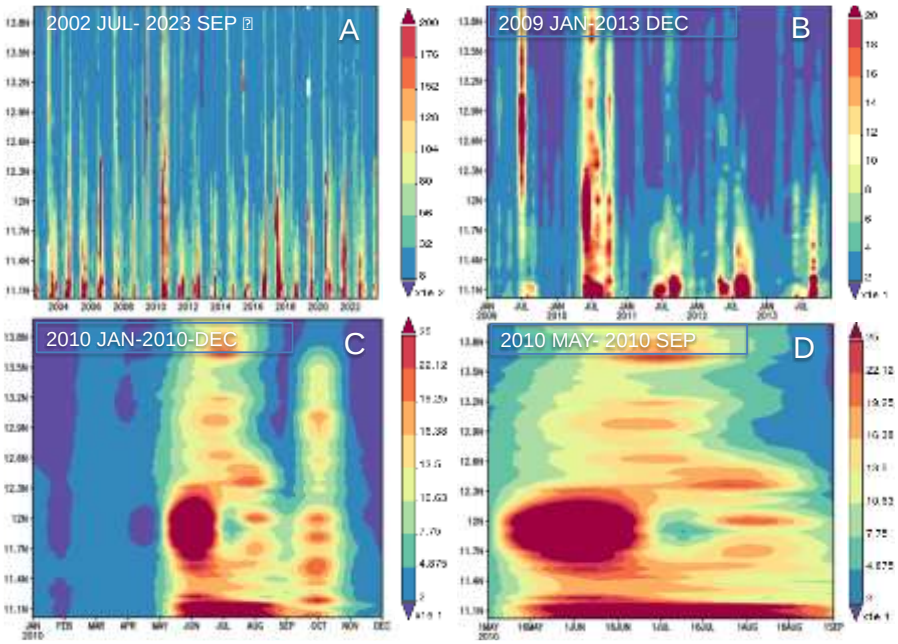

Figure 20: Hovmöller longitude-averages of chlorophyll concentrations (mg m^{-3}) east of the Lesser Antilles at 11^0N, 60^0W, 14^0N, 61^0W, shown in Figure 1 as Site A. Figure 20A: July 2002 to September 2023; Figure 20B: January 2009 to December 2013; Figure 20C: January to December 2010; Figure 20D: May to September 2010.

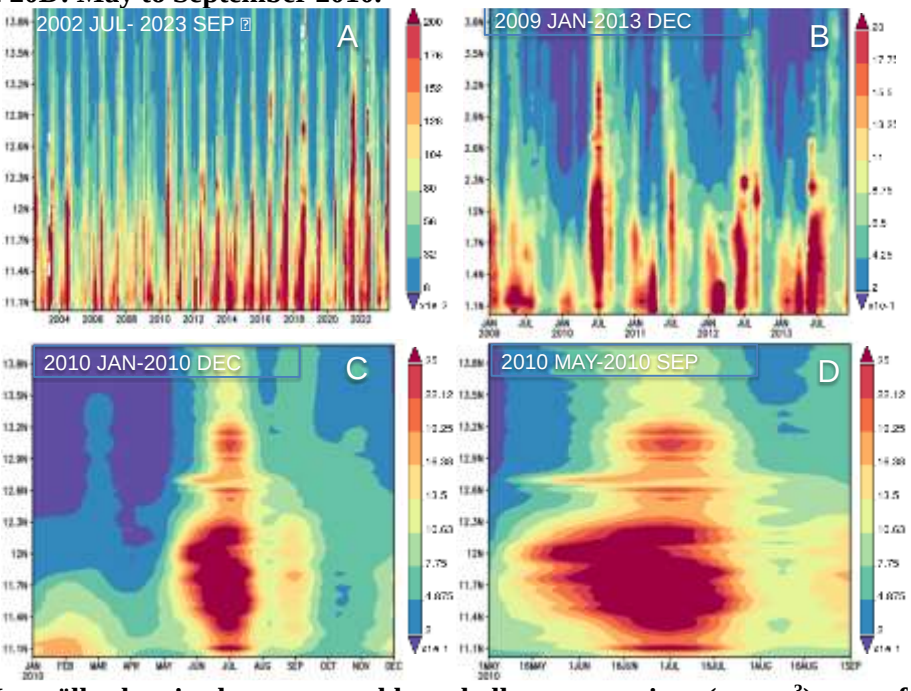

Figure 21: Hovmöller longitude-averages chlorophyll concentrations (mg m^{-3}) west of the Lesser Antilles at 11^0N, 63^0W and 14^0N 64^0W; it is shown in Figure 1 as Site B. Figure 21A: July 2002 to September 2023; Figure 21B: January 2009 to December 2013; Figure 21C: January to December 2010; Figure 21D: May to September 2010.

The observations east of the Lesser Antilles are compared with observations west of the Lesser Antilles and are shown in Figure 21. Significant differences are recognized in the chlorophyll concentrations, as shown in Figure 21A, that is due to the impact of water from the Orinoco and the contribution from the upwelling regime along the Venezuela coast. Extended views in Figure 21C and Figure 21D show a patch that covers the same time sequence as the images shown in Figure 20 for the eastern side of the Lesser Antilles. This comparison allows an estimate of the displacement of the surface patch. Considering that the eastern patch moved westward and arrived somewhere around 20 June, it would have drifted at approximately 8 to10 cm s^{-1} (~0.1m s^{-1}).
Another comparison of the two sites A and B is shown for January to December 2017 in Figure 22 where figures A' and B' are the corresponding images at higher temporal resolution for the period May to September 2017. Site A east of the Lesser Antilles shows that chlorophyll maxima are in June at around 12^0N. In the following months, the maximum values drift to lower latitudes and in November it is found at around 11.1^0N.

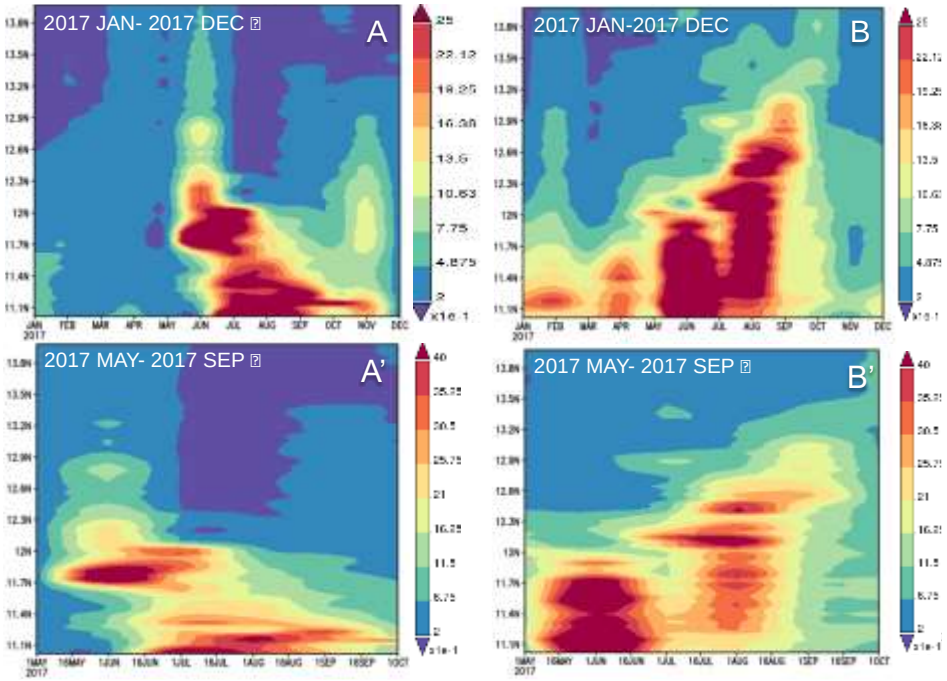

Figure 22: Comparison of Hovmöller longitude-averaged chlorophyll concentrations (mg m^{-3}) of Site A east of the Lesser Antilles at 11^0N, 60^0W and 14^0N, 61^0W and Site B west of the Lesser Antilles at 11^0N, 63^0W and 14^0N 64^0W. Below A and B, are the corresponding images A' and B' covering May to September 2017.

The expanded scale in Figure 22A' shows that two separate maxima occur in 2017, although they appear at different time-space scales. The western Site B also shows two major chlorophyll maxima whereby the first appears around June, and the second begins in August, but it shifts to around 12^0N in September. The comparison of the two sites show opposite direction in progression of chlorophyll concentrations that must have different causes and seem to be related to the passing of rings and their remnants east of the Lesser Antilles. Aside from ring remnants, upwelling and river discharge are major causes for elevated chlorophyll concentrations on the western side of the Lesser Antilles. Thus, the distribution pattern observed at the western part of the Lesser Antilles is not necessarily only a result of patterns that are transferred from the eastern section.

Destruction of rings

The image interpretation showed that ring structures at the surface are not recognized past 20^{0}N, and it seems that rings stall for a noticable time between Trinidad and Barbados where they start to decay. Not very much is known about the mechanism that causes ring decomposition but an image sequence shown in Figure 24 demonstrates that fast changes may occur while a ring is in the proximity of the Lesser Antilles. On 27 March, a ring reached the region east of Trinidad, and from 10 April it was well recognized until 19 April. On 28 April the ring started to lose its circular surface appearance, and on 4 May, the original ring was stretched into an elongated water mass that continoued to travel in a northwest direction. While the southwest part of the decaying ring transited through the passages north of Trinidad and south of St. Vincent, the northern decaying part of the ring reached the passages between Martinique and Guadeloupe. Residuals of the ring arrived on 13 May at the latitude of St. Bathélemy and were still recognized on 25 May before moving in a northwest direction.

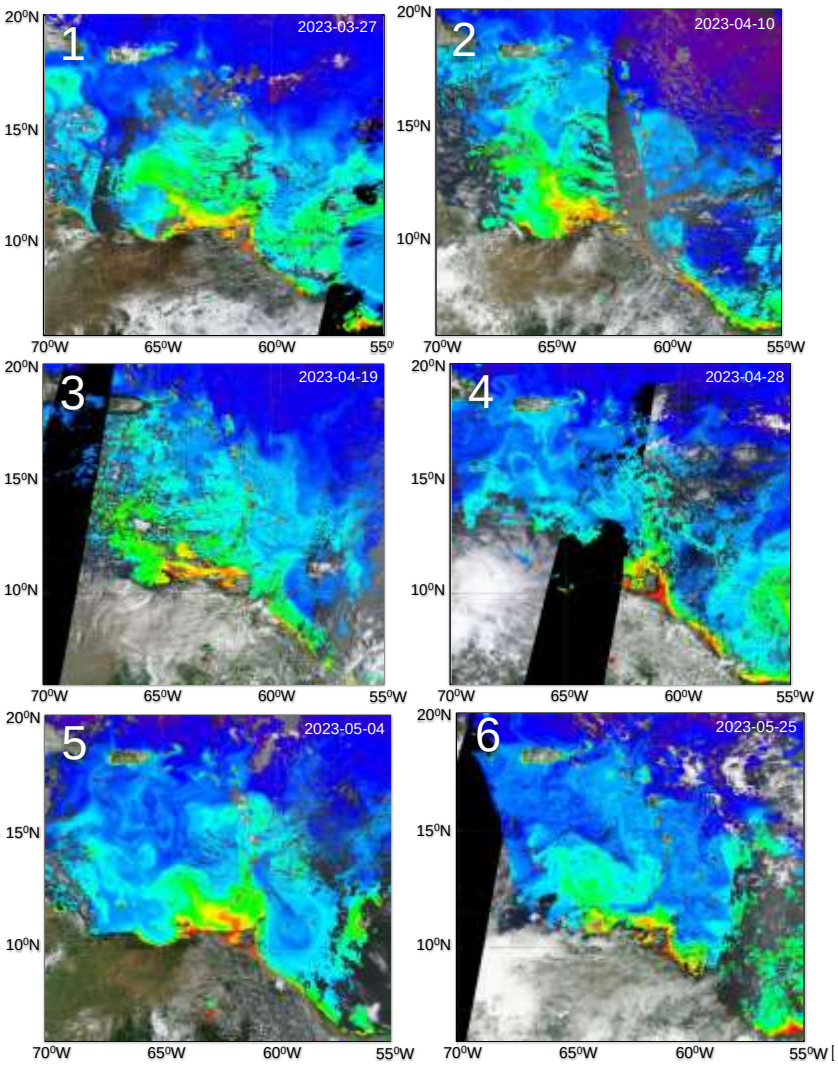

Figure 23: Arrival and destruction of a ring's surface in the vicinity of Trinidad on 27 March to 25 May. The area of the images covers Site 3 as shown in Figure 1 at 5^{0}N, 55^{0}W and 20^{0}N, 70^{0}W.

Another image sequence obtained in September 2023 permitted the retrieval of details on the progressive changes of a ring. The ring stalled east of Trinidad with its center at $10^0$44'N, $58^0$55'W, and its changes were observed with images of which three are shown in Figure 24. Image 24C shows that the diameter of the ring was about 420 km.

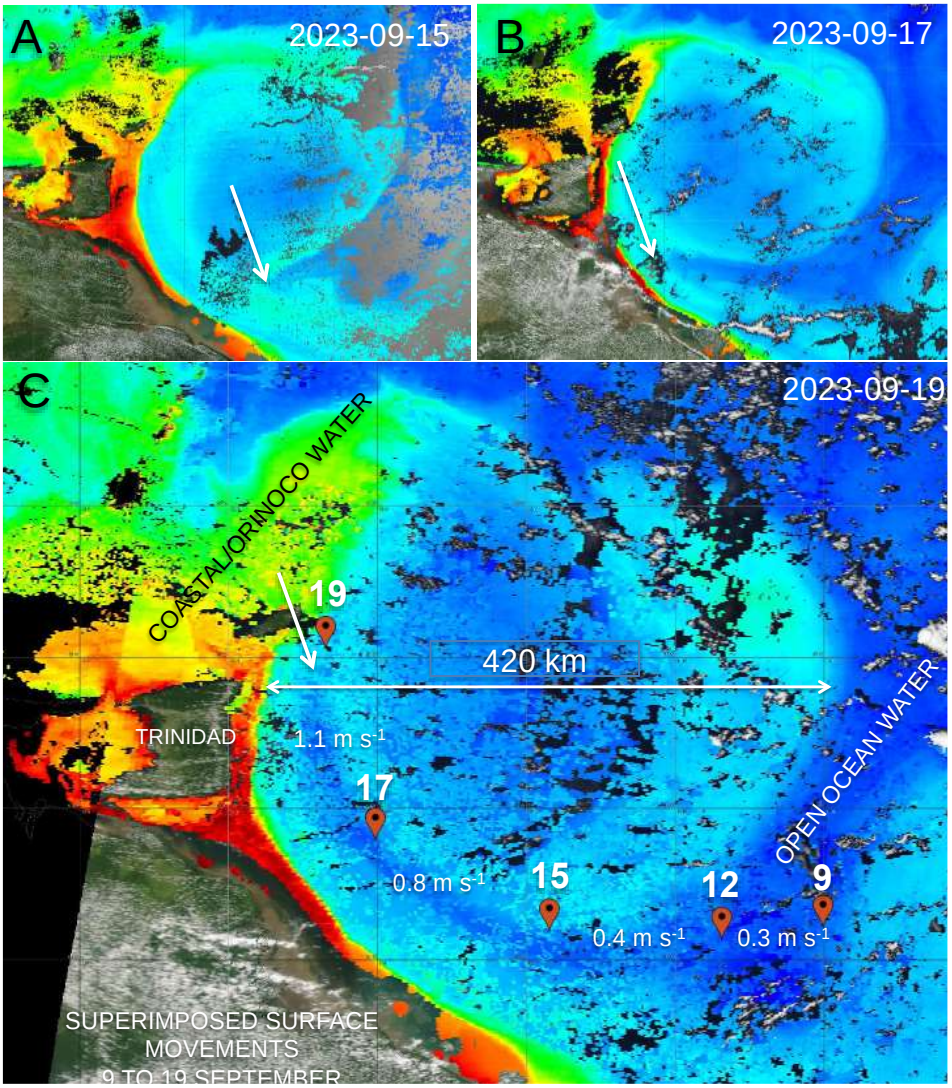

Figure 24: Stalled ring east of Trinidad with the center at $10^0$44'N and $58^0$55'W. 24A: 15 September 2023; 24B: 17 September 2023; 24C: The image from 19 September 2023 shows the diameter of the ring and superimposed markers for the location and date of observation from 9 to 19 September 2023. The white arrows in Figures A, B and C show the edge of the entrapped ocean water and its displacement that was used to estimate the azimuthal velocity of entrapment.

The image sequence also allowed an estimate of azimuthal speed of the surface water that was dragged from the open ocean into the outer periphery of the ring. Contrary, on the western part of the ring, a mixture of coastal water and effluent from the Orinoco was incorporated into the outer part of the ring. Intrusion of open ocean water starts at the ring's eastern margin around 9 September at a velocity of approximately 0.3 m s^{-1}, but the speed accelerated to about 1.1 m s^{-1} once the water reached the western

outer part of the ring. Thus, the water close to Trinidad is a mixture of open ocean water, Orinoco effluent with contributions from the Essequibo (Wilson, 2008), and Amazon ring water. This mixture establishes significant horizontal gradients and seasonal fluctuations in temperature, salinity and watercolor. The observations on this ring also provided information on the duration of ring demise because the ring was first recognized east of Trinidad on 10 September 2023 but its surface signature was lost on 25 November. That indicates that after stalling, the destruction of this ring's surface may be in the neighborhood of about 70 days.

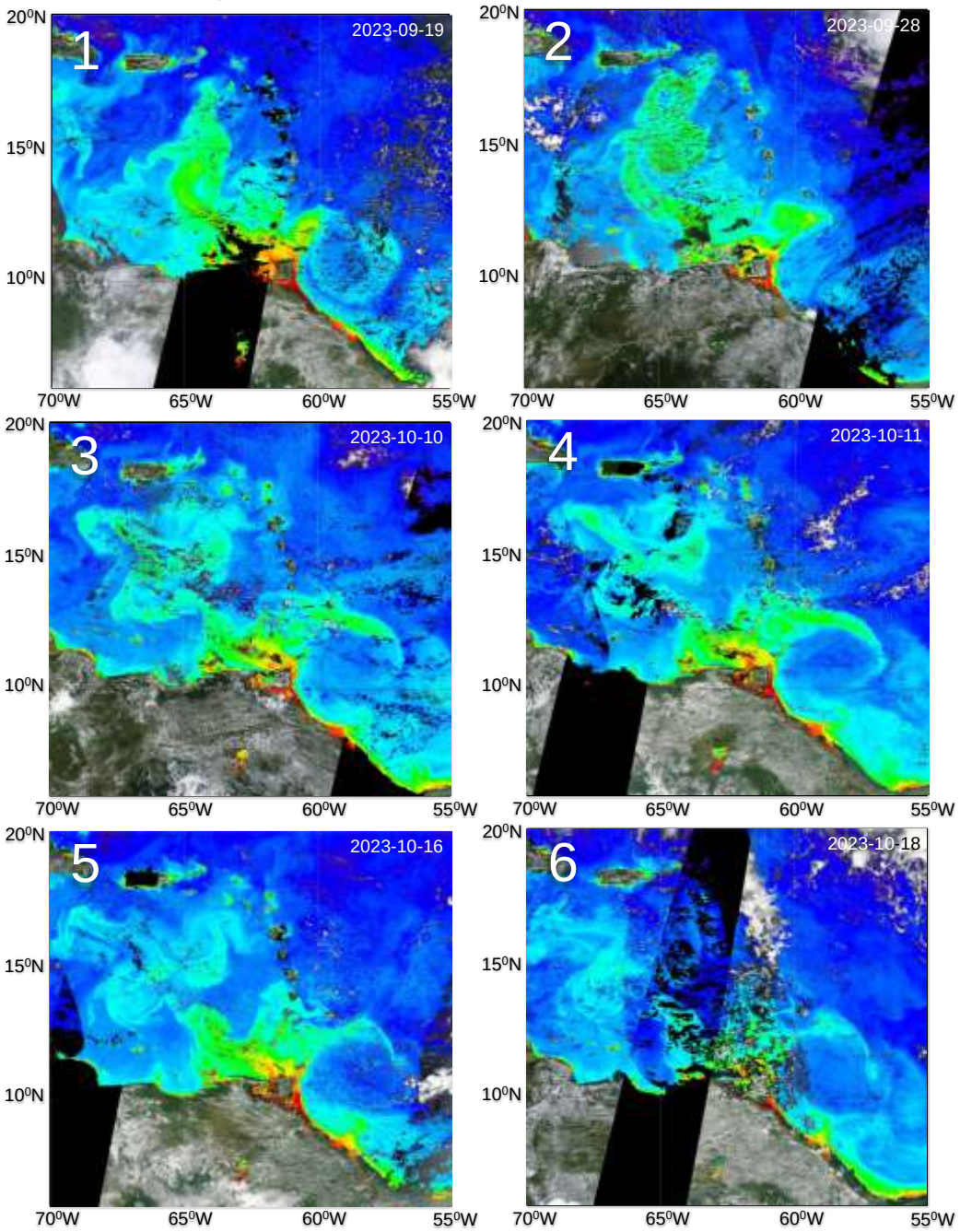

Figure 25: Changes in surface appearance of a ring from 19 September to 18 October 2023. The area of the images covers Site 3 as shown in Figure 1 at 5⁰N, 55⁰W and 20⁰N, 70⁰W.

The degredation of the ring shown in Figure 24 continued in September, and Figure 25 shows with another image sequence that the ring started to dispatch some of its ring water through the southern island passages. After moving through the passage, further interaction with water from the upwelling regime around the northern part of Trinidad takes place. As seen in Figures 25.3 to 25.6, the resulting mixture is responsable for the formation of a strong color gradient in surface water northwest of Trinidad.

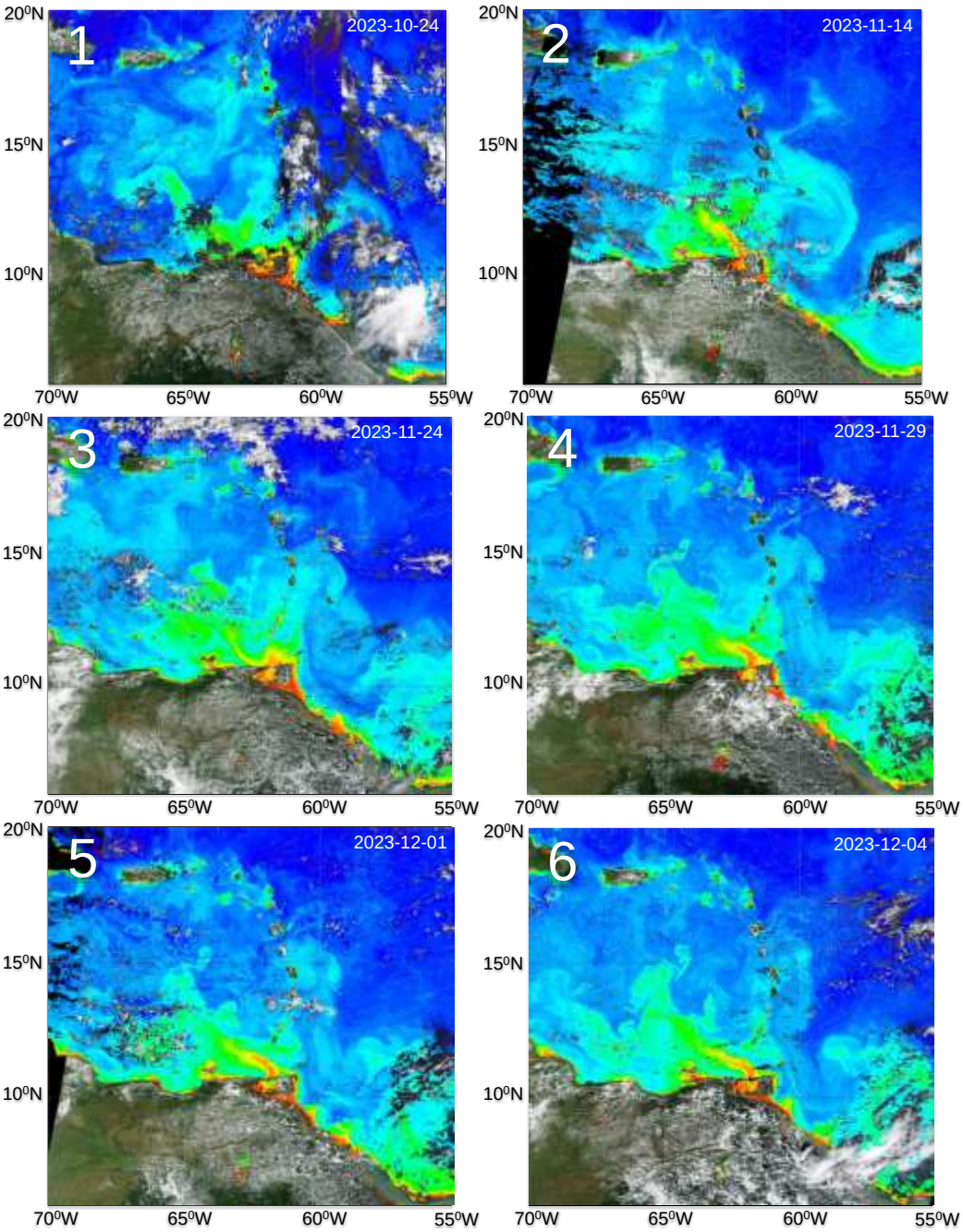

Figure 26: Changes in surface appearance of a ring from 24 October 2023 to 4 December 2023. The area of the images covers Site 3 as shown in Figure 1 at 5⁰N, 55⁰W and 20⁰N, 70⁰W.

Figure 26 shows that the ring structure is still recognized on 24 October, and as the direction of the Orinoco plume indicates, the ring incorporates additional coastal water in its outer periphery. On 30 October (image not shown), the ring started to decompose and dragged the incorporated coastal water offshore farther north, while the Orioco plume redirected back ~~to~~ northwest through the Bay of Paria. On 14 November the ring is still recognized with its center at $11^0$49'N, ~~and~~ $59^0$21'W, close to the south of Barbados, but the northern part of the diminishing ring reaches Dominica while the western segment starts to pass between Grenadine Islands and St. Vincent. Around 23 November, the ring loses its surface manifestations, and on 26 November, the remnants of the ring reach Dominica, and on 3 December, reached as far as Guadeloupe.

Interaction of ring water with Orinoco effluent east of Trinidad is further documented with a ring that arrived east of Trinidad. The image sequence shown in Figure 27 details the interaction of Orinoco effluent and the western edge of the ring on 25 to 28 December 2021 when densely colored water passed trough the Paria Bay and also spread along the east coast of Trinidad. This is the time when the ring incorporated Orinoco water in the outer ring periphery. However, on 27 December, ring water seems to pressure the Orinoco plume towards the west and a weak signal of the Orinoco plume is visible. Once the ring continues its journey to the north, the Orinoco plume is fully visible on 31 December as seen in the images obtained on 5 and 6 January 2022.

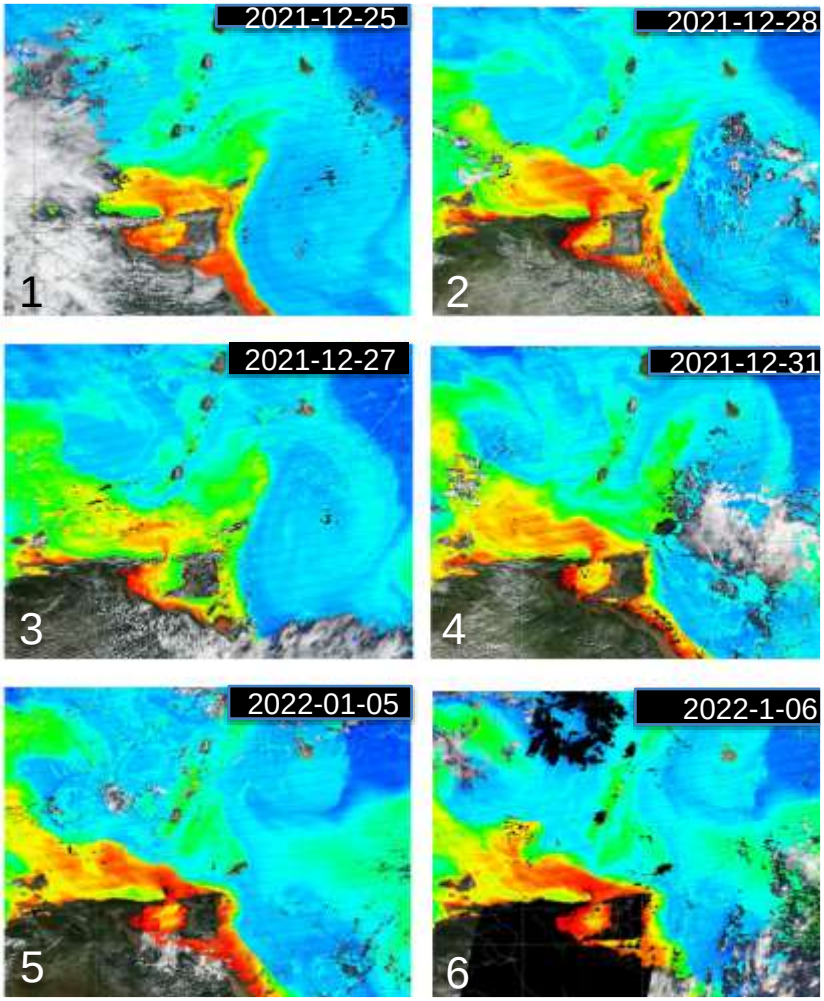

Figure 27: Interaction of the ring periphery with the Orinoco effluent as observed from 25 December 2021 to 6 January 2022.

The observations in this study showed that once rings are stalled upon arrival at low bathymetry, close to Trinidad and Barbados, the upper part of the ring modifies its surface characteristics. The outer ring structure broadens until it begins to disperse by action of the westward flow of Atlantic surface water. There seems to be a common mechanism for ring destruction that is explained with a ring that stalled, shown in Figure 28.

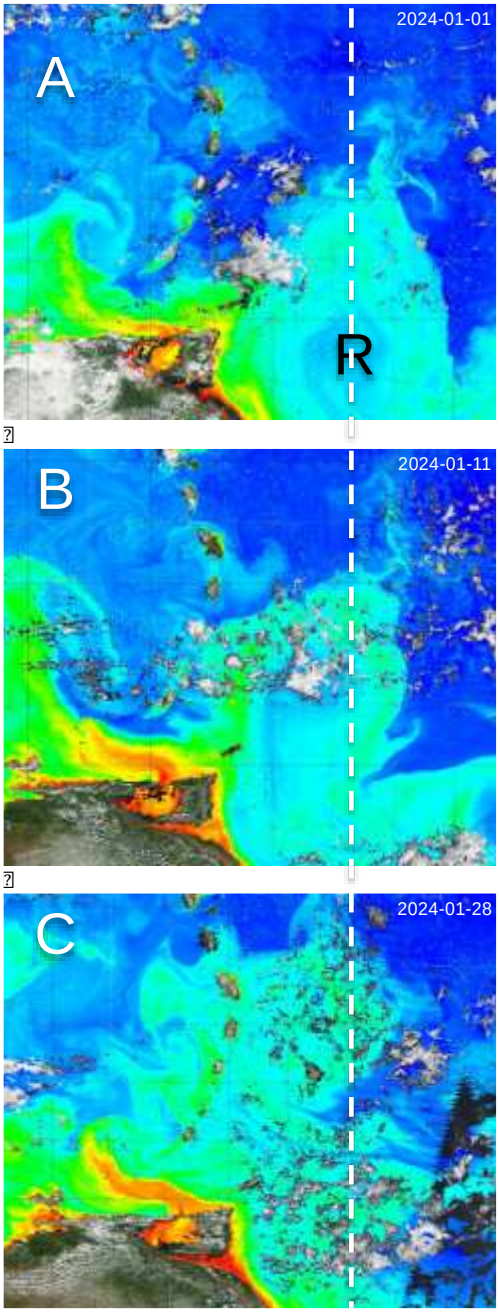

Figure 28: Decay and destruction of a ring observed with selected images during January 2024. The ring center of the stalled ring in image A shows the reference line (R) in estimating the displacement of ring remnants in Figures B and C.

The tracking of ring and ring remnants shows that the northern part of the ring translates northwest at about 0.1 m s^{-1}, whereas ring remnants at the western boundary of the ring start to move through the southern island passages at about 0.15m s^{-1}. This process continues while the inflowing Atlantic water to the Caribbean starts to further pressure surface remnants in a westward direction through the passages. However, the major transport of residual ring water passes through the channels south of Guadeloupe and Dominique. An estimate for the time of ring destruction is based on tracking of rings and their remnants, and indicates that the destruction of surface ring pattern can take place within four weeks.

CONCLUSIONS

The study revealed the complexity of surface water that flows towards the Lesser Antilles and eventually passes through their channels. This study gained with image interpretation additional information on rings with respect to their formation, life duration and destruction. By monitoring the retroflection of the North Brazil Current (NBC), the region where ring formation is observed, it was shown that the retroflection could move from its southern position at around 6^0N during summer to around 9^0N in late autumn. However, the retroflection may fluctuate once a ring has been released. After separation from the retroflection, a ring fluctuates as well, and the amplitude of ring motion is highest close to the retroflection, but it is reduced once the ring starts to translate away from the retroflection. The observed rings have a lifespan of around 70 to 100 days and they may have a displacement velocity of about 0.15 m s^{-1} once they arrive east of Trinidad. However, formation and translation of rings show temporal and spatial irregularity in ring appearance, and fluctuations in intensity seem to be a common feature. During their translation, rings interact with costal water, and the western side of the outer ring periphery has in some cases spectral properties that are closer to Case 2 water than to Case 1 water.

Upon arrival close to Trinidad, there is additional interaction of ring water with effluent from the Orinoco River. Part of this mixture enters the passage to the Gulf of Paria while another part is transported farther north as remnants from ring decay. The northern decaying part of rings may reach the passages between Martinique and Guadeloupe but rarely extend to the latitude of St. Bathélemy. During the decay phase, open ocean water starts to enter the ring's eastern margin at a velocity of approximately 0.3 m s^{-1}, but the azimuthal speed of surface water can accelerate to about 1.1 m s^{-1} once ocean water reaches the western outer part of the ring. The inflowing Atlantic water to the Caribbean starts to pressure surface remnants in a westward direction through the passages, but image interpretation shows that the major transport of residual surface ring water appears mainly south of Guadeloupe and Dominique. Stalled rings in the vicinity of Trinidad indicate that destruction in the surface distribution pattern of a ring may occur within four week.

The image interpretation on the mixing of ring water and the Orinoco effluent demonstrated that the resulting mixture enters partly through the passage to the Gulf of Paria while another part is transported farther north. This mixture of river effluent and ring water adds to the nutrient pool of surface water and would explain the observations by Bonilla et al. (1993) that the Orinoco effluent and low-salinity coastal waters initiate eutrophication in fertilizing large areas of the eastern Caribbean Sea. This may also explain the strong color gradients and changes in optical properties observed. However, aside from eutrophication, other processes may be responsible for changes in color and may be of multiple origins although eutrophication by the dispersal of the ring water and its mixture is the most plausible reason.

ACKNOWLEDGEMENT

The author is Fulbright Alumnus at Ateneo University de Manila and at the University of the Bahamas. Analyses and visualizations used in this study were produced with the Giovanni online data system, developed and maintained by NASA GES DISC. The MODIS mission scientists and associated NASA personnel are acknowledged for the production of the data used in this research effort.

REFERENCES

Acker JG and Leptoukh G (2007). Online analysis enhances use of NASA earth science data. *Eos, Transactions American Geophysical Union*, **88** (2) 14–17. DOI: *Available at: https://doi.org/10.1029/2007EO020003.*

Bonilla J, Senior W, Bugden J, Zafiriou O and Jones R (1993). Seasonal distribution of nutrients and primary productivity on the Eastern Continental Shelf of Venezuela as influenced by the Orinoco River. *Journal of Geophysical Resea*rch **98** 2245-2257.

Chérubin LM, Garavelli L (2016). Eastern Caribbean circulation and island mass effect on St. Croix, US Virgin Islands: A mechanism for relatively consistent recruitment patterns. PLOS ONE 11(3): e0150409. *Available at: https://doi.org/10.1371/journal.pone.0150409*

Cruz Gómez RC and Bulgakov SN (2007). Remote sensing observations of the coherent and non-coherent ring structures in the vicinity of Lesser Antilles. *Annales Geophysichae* **25** 331–340, https://doi.org/10.5194/angeo-25-331-2007, 2007.

Del Castillo CE, Coble PG, Morell JM, Lapez JM and Corredor JE (1999). Analysis of the optical properties of the Orinoco River plume by absorption and fluorescence spectroscopy. *Marine Chemistry* **66** 35-51.

Didden N, and Schott F, 1993. Eddies in the North Brazil Current Retroflection region observed by Geosat altimetry. *Journal of Geophysical Research* **98** 20 121–20,131.

Duncan CP, Schladow SG and Williams WG (1982). Surface currents near the Greater and Lesser Antilles. *International Hydrographic Review*, Monaco. **LIX** (2) 67-78.

Fratantoni DM and Glickson DA (2002). North Brazil Current ring generation and evolution observed with SeaWiFS. *Journal of Physical Oceanography* **32** 1058–1074 /1058:NBCRGAS2.0.CO;2.

Fratantoni DM, Johns WE and Townsend TL (1995). Rings of the North Brazil Current: their structure and behavior inferred from observations and a numerical simulation. *Journal of Geophysical Research.* **100** (C6) 10,633–10,654.

Frantantoni DM and Richardson PL (2006). The evolution and demise of North Brazil Current rings. *Journal of Physical Oceanography* **36** 1241-1264.

Garzoli S, Field A and Yao Q (2003). North Brazil Current rings and the variability in the latitude of retroflection. In: Interhemispheric Water Exchange in the Atlantic Ocean, edited by Goni G and Malanotte-Rizzoli P, *Elsevier Oceanography Series*, Elsevier, Amsterdam. **68** 357–374.

Goni G and Johns WE (2001). A census of North Brazil Current rings observed from T/P altimetry: 1992–1998. *Geophysical Research Letters* **28** (1), 1–4.

Hu C, Montgomery ET, Schmitt RW and Müller-Karger FE (2004). The dispersal of the Amazon and Orinoco River water in the tropical Atlantic and Caribbean Sea: Observation from space and S-PALACE floats. *Deep-Sea Research Part II Topical Studies in Oceanography*. **51** (10-11) 1151-1171 DOI:10.1016/j.dsr2.2004.04.001.

Johns E, Wilson WD and Molinari RL (1999). Direct observations of velocity and transport in the passages between the Intra-Amearicas Sea and the Atlantic Ocean, 1984–1996. *Journal of Geophysical Research.* **104** (C11).

Johns EM, Muhling BA, Perez RC, Muller-Karger FE, Melo N, Smith RH, Lamkin JT, Gerard, TL and Malca E (2014). Amazon River Water in the Northeastern Caribbean Sea and Its Effect on Larval Reef Fish Assemblages during April 2009. *Marine Science Faculty Publications*. 1052. https://digitalcommons.usf.edu/msc_facpub/1052

Johns WE, Lee TN, Schott FA, Zantopp RJ and Evans RH (1990). The North Brazil Current retroflection: seasonal structure and eddy variability. *Journal of Geophysical Rese*arch **95** (C12), 22,103–22,120.

Johns WE, Townsend TL, Fratantoni DM and Wilson WD (2002). On the Atlantic inflow to the Caribbean Sea. *Deep-Sea Research Part I*. **49** 211-243.

Lumpkin R and Garzoli SL (2005). Near-surface circulation in the tropical Atlantic Ocean. *Deep-Sea Res. II*. **52** 495–518.
Müller-Karger FE, McClain CR and Richardson PL (1988). The dispersal of the Amazon's water. *Nature*. **333** 56–59.
Müller-Karger FE, McClain CR, Fisher TR, Esaias WE and Varela R (1989). Pigment distribution in the Caribbean Sea: Observations from space. *Progress in Oceanography*. **23** 23-64.
Richardson PL (2005). Caribbean Current and eddies as observed by surface drifters. *Deep-Sea Research II.* **52** (2005) 429–463.
Richardson PL, Hufford GE, Limeburner R and Brown WS (1994). North Brazil Current Retroflection Eddies. *Journal of Geophysical Research.* **99** (C3), 5081–5093.
Rueda-Roa DT and Müller-Karger FE (2013). The southern Caribbean upwelling system: Sea surface temperature, wind forcing and chlorophyll concentration patterns. *Deep-Sea Research I.* **78** (2013) 102–114.
Stalcup MC and Metcalf WG (1972). Current measurements in the passages of the Lesser Antilles. *Journal of Geophysical Research*. **77** 1032–1049.
Szekielda KH (2023). Wakes and Thermal Anomalies in the Lesser Antilles Surface Water. *International Journal of Geology, Earth and Environmental Sciences*. **13** 100-132 ISSN: 2277-208.
Wilson B (2008). Distributions of ostracod (Crustacea) biofacies on the continental shelf off south-east Trinidad, western central Atlantic Ocean, suggest the location of an offshore river- induced front within the Orinoco Plume. *Senckenbergiana lethaea*. **88** (2) 199 – 211.
Wilson WD and Johns WE (1997). Velocity structure and transport in the Windward Islands passages. *Deep-Sea Research* **44** (3), 487–520.

***Copyright**: © 2024 by the Author, published by Centre for Info Bio Technology. This article is an open access article distributed under the terms and conditions of the Creative Commons Attribution (CC BY-NC) license [https://creativecommons.org/licenses/by-nc/4.0/], which permit unrestricted use, distribution, and reproduction in any medium, for non-commercial purpose, provided the original work is properly cited.*